CrossMark

Annual Phytoplankton Primary Production Estimation in a Temperate Estuary by Coupling PAM and Carbon Incorporation Methods

Jérôme Morelle [1,2] · Mathilde Schapira [3,4] · Francis Orvain [1,2] · Philippe Riou [3] · Pascal Jean Lopez [2] · Olivier Pierre-Duplessix [3,4] · Emilie Rabiller [3] · Frank Maheux [3] · Benjamin Simon [3] · Pascal Claquin [1,2]

Abstract

Phytoplankton primary production varies considerably with environmental parameters especially in dynamic ecosystems like estuaries. The aim of this study was to investigate short-term primary production along the salinity gradient of a temperate estuary over the course of 1 year. The combination of carbon incorporation and fluorescence methods enabled primary production estimation at short spatial and temporal scales. The electron requirement for carbon fixation was investigated in relation with physical-chemical parameters to accurately estimate primary production at high frequency. These results combined with the variability of the photic layer allowed the annual estimation of primary production along the estuary. Phytoplankton dynamics was closely related to salinity and turbidity gradients, which strongly influenced cells physiology and photoacclimatation. The number of electrons required to fix 1 mol of carbon (C) was ranged between 1.6 and 25 mol electron mol C^{-1} with a mean annual value of 8 ± 5 mol electron mol C^{-1}. This optimum value suggests that in nutrient replete conditions like estuaries, alternative electron flows are low, while electrons transfer from photosystem II to carbon fixation is highly efficient. A statistical model was used to improve the estimation of primary production from electron transport rate as a function of significant environmental parameters. Based on this model, daily carbon production in the Seine estuary (France) was estimated by considering light and photic zone variability. A mean annual daily primary production of 0.12 ± 0.18 g C m^{-2} day^{-1} with a maximum of 1.18 g C m^{-2} day^{-1} in summer was estimated which lead to an annual mean of 64.75 g C m^{-2} $year^{-1}$. This approach should be applied more frequently in dynamic ecosystems such as estuaries or coastal waters to accurately estimate primary production in those valuable ecosystems.

Keywords High frequency · Electron requirement for carbon fixation · Electron transport rate (ETR) · Seine estuary

✉ Pascal Claquin
pascal.claquin@unicaen.fr

1 Normandie Université, Université de Caen Normandie, F-14032 Caen, France

2 UMR Biologie des ORganismes et Ecosystèmes Aquatiques (BOREA), Muséum National d'Histoire Naturelle, CNRS-7208, IRD-207, Sorbonne Université, Université Caen-Normandie, Université des Antilles, Esplanade de la paix, F-14032 Caen, France

3 Ifremer, LER/N, Avenue du Général de Gaulle, 14520 Port-en-Bessin, France

4 Present address: Ifremer, LER/MPL/NT, Rue de L'Ile d'Yeu, BP 21105, 44301 Nantes CEDEX 03, France

Introduction

Phytoplankton primary production (PPP) is one of the most important processes in aquatic ecosystems which is at the base of the marine trophic network (Pauly and Christensen 1995; Chen and Borges 2009; Cloern et al. 2014). It is therefore essential to accurately estimate the PPP to understand, apprehend, and manage the ecosystems. However, PPP varies considerably with environmental parameters (Cloern 1996; Pannard et al. 2008), including light availability (Falkowski and Raven 1997; Anning et al. 2000; Macintyre et al. 2002), nutrient concentrations (Dortch and Whitledge 1992; Lohrenz et al. 1999; Tillmann et al. 2000; Claquin et al. 2010), and temperature (Davison 1991; Falkowski and Raven 1997; Shaw and Purdie 2001; Claquin et al. 2008). The most commonly used methods for in situ estimation of PPP are carbon isotopes (^{14}C or ^{13}C) incorporation (Babin et al. 1994; Cloern et al. 2014) methods. Carbon isotope methods are sensitive,

Springer

but the long incubation periods required are a disadvantage for accurate estimations at small spatial and temporal scales. The PAM (pulse amplitude modulated) fluorometer method based on variations in the fluorescence emitted by the photosystem II (PSII) during photosynthesis allows rapid measurements of photosynthetic parameters (Parkhill et al. 2001; Kromkamp and Forster 2003; Napoléon and Claquin 2012). In contrast to the carbon incorporation method, which gives the rate of photosynthetic carbon incorporated, the PAM method gives access to the electron transport rate (ETR) from the PSII (Kolber and Falkowski 1993; Barranguet and Kromkamp 2000). The combination of these both methods allows to estimate the number of electrons required to fix 1 mol of carbon. Therefore, PPP can be estimated at small spatial and temporal scales as a function of the environmental parameters (Napoléon and Claquin 2012; Lawrenz et al. 2013; Hancke et al. 2015), and previous studies have shown that the estimation of the PPP by this way was as accurate than other traditional incubation methods such as carbon isotopes incorporation or oxygen measurements (Hartig et al. 1998; Barranguet and Kromkamp 2000; Kromkamp and Forster 2003; Morris and Kromkamp 2003).

The variability of environmental factors that could influence PPP is particularly high in dynamic ecosystems such as estuaries (Underwood and Kromkamp 1999; Cloern et al. 2014). These dynamic ecosystems are characterized by high variability at seasonal and tidal scales. Located at the interface between land and sea, estuaries are influenced by the freshwater outflow from the river and the marine water inflow from the tide. These ecosystems are known to play therefore important role in biogeochemical cycles (Chen and Borges 2009). Along the estuaries, PPP is affected by several gradients (i.e., salinity, turbidity, nutrient concentrations, and light availability) caused by the dilution of the marine water brought by the tide with fresh water from the river (Kimmerer et al. 2012). PPP is usually the lowest within the maximum turbidity zone (MTZ) created by tidal asymmetries in particle transport brought about by the effect of gravitational circulation on tidal flows (Sanford et al. 2001) which induce low light penetration, salt stress, and cell lysis (Goosen et al. 1999). Despite the large number of studies on temporal variations of PPP in estuaries, very few studies have been conducted at small spatial and temporal scales (Parizzi et al. 2016), and many large estuaries are still poorly studied. This is the case of the Seine estuary, which represents the largest outflow into the English Channel. Thus, the aims of this study were the following: (1) to investigate monthly the time and space dynamics of photosynthetic parameters along the estuary by using high-frequency measurements during 1 year and identify the main factors controlling those parameters; (2) to explore the relationships between ETR and C fixation as a function of environmental factors; (3) to apply the multi-factorial relationships obtained on the whole ETR data set in order to estimate PPP from daily to annual scale.

Methods

Study Site

The Seine River and its estuary drain a watershed covering 76,260 km^2. After Paris, the river flows northwest and drains its water into the English Channel. Located 202 km from Paris (the kilometric scale of the Seine River is set at 0 km in the center of Paris), the weir at Poses (Fig. 1) represents the upper limit of the tidal propagation in the Seine estuary. The annual average river discharge at Poses is 436 m^3 s^{-1} with a flood period extending from December to April when the discharge reaches 1200–2500 m^3 s^{-1} and a low-flow period with a discharge of around 250 m^3 s^{-1} (Data GIP Seine-Aval, 2008; 2011). In the oligohaline part, salinity ranges from 0.5 to 5; in the mesohaline part, salinity ranges from 5 to 18; in the polyhaline part, from 18 to 30; and in the euhaline part, salinity is above 30. The Seine estuary is a macrotidal type estuary, with a tidal amplitude ranging from 3 to 7 m at Honfleur and 1 to 2 m at Poses. The mean residence time in the estuary varies between 17 and 18 days for a discharge of 200 m^3 s^{-1} at Poses and between 5 and 7 days for a discharge of 1000 m^3 s^{-1} (Brenon and Le Hir 1999; Even et al. 2007). The tide in the Seine estuary is characterized by flattening at high tide lasting more than 2 h due to the deformation of the tidal wave during the propagation at shallow depths (Brenon and Le Hir 1999; Wang et al. 2002). The flow is asymmetric in favor of the flood and this trend increases as the tide propagates up the estuary. Seasonally, water temperature ranges between 25 °C in summer and 7 °C in winter with differences of less than 1 °C along the longitudinal profile and a weak vertical gradient (Data GIP Seine-Aval, 2008; 2011). The MTZ, containing up to 2 g L^{-1} of suspended particulate matter (SPM), is most often located between Honfleur and Tancarville, but can move upstream depending on the intensity of the tide and river discharge. During winter flood events, the MTZ can be flushed out into the Seine Bay (Etcheber et al. 2007; Garnier et al. 2010).

Sampling Strategy

Sampling was conducted monthly from January to December 2015 onboard the Ifremer ship "Delphy" at eight sampling sites scattered along the salinity gradient (Fig. 1). The sites were distributed from the euhaline zone (site 1) to the oligohaline zone (site 8). In order to sample a steady waterbody along the estuary, sampling was performed every month in spring tides conditions (tidal coefficient 90) during daylight and during the flattening of the high tide, which, in these conditions, lasts up to 3 h along the Seine estuary. Along the salinity gradient, from site 1 to site 8, P/E curves were performed at high frequency with 5-min intervals in subsurface water using the PAM method providing almost 40
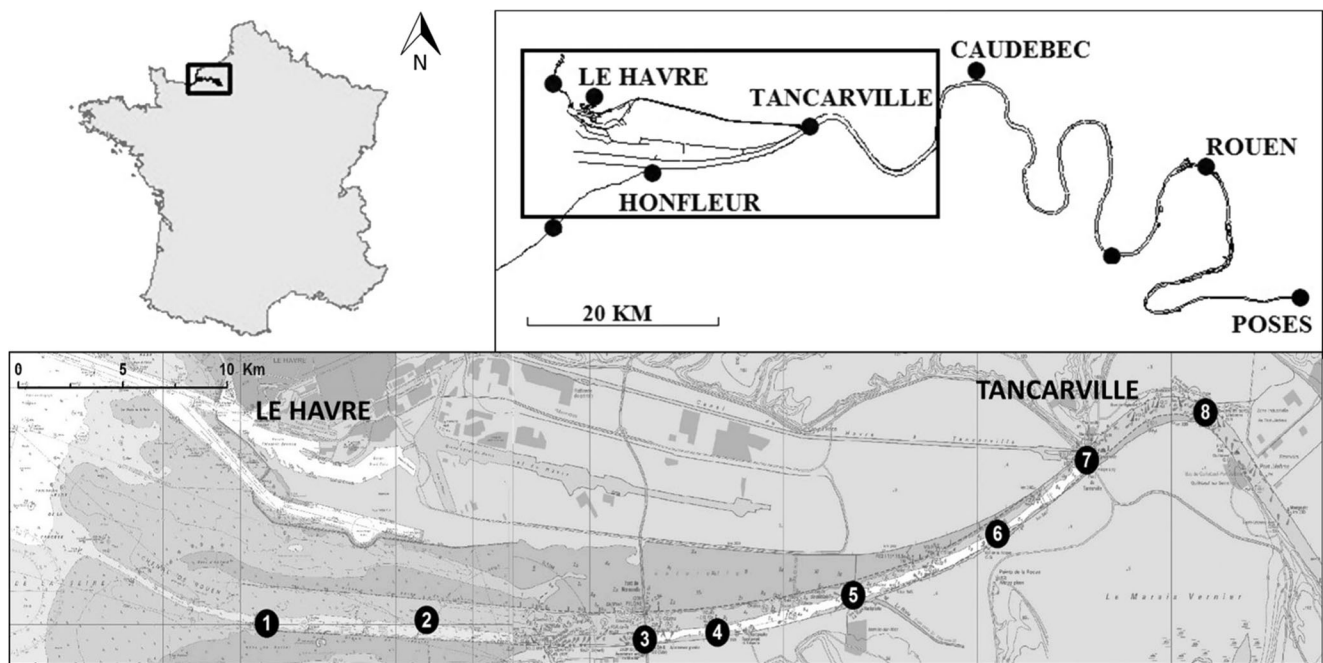
Fig. 1 Map of the Seine estuary (longitude: 0.2327, latitude: 49.4326 (WGS84)—Normandy, France) showing the study area. Poses is the upper limit of tidal propagation. The lowest map is a close-up of the square site in the right upper map corresponding to the sampling area. The sampling transect from site 1 to site 8 followed the salinity gradient from the euhaline zone (site 1) to the oligohaline zone (site 8). The sites were sampled monthly throughout 2015

distinct measurements along the transect. The device already used in (Napoléon et al. 2012, 2014) that made it possible to carry out these measurements at high frequency is presented in Fig. 2. In parallel, salinity (measured using the Practical Salinity Unit; PSU), turbidity (measured using the Nephelometric Turbidity Unit; NTU), and temperature (°C) were recorded in vertical profiles at each site using a SBE 19-plusVD CTD (Seabird) from the sub-surface down to 1 m above the water-sediment interface (WSI). At each sampling site, water was sampled from the sub-surface (i.e., 1 m) with a pump for analysis of the physical-chemical (nutrients, SPM) and biological parameters (chl$a$, F_V:F_M). At sites 2, 4, 6, and 8, sampling was also conducted from 1 m above the WSI with a 5-L Niskin bottle and at these sites, a part of the water samples from sub-surface was used to estimate primary production using the ^{13}C incorporation method.

Physical-Chemical Parameters

Nutrients

To determine the concentration of nutrients (PO_4^{3-}, NO_3^-, NO_2^-, NH_4^+, and $Si(OH)_4$), 100 ml water samples were pre-filtered through a 48-μm Nylon Mesh (Sefar Nitex 03–48/31–102 cm; Open area %: 30) directly from the Niskin bottle in order to already eliminate a major part of the particles (Aminot and Kérouel 2004, 2007) and stored at 4 °C until analysis. For the determination of concentrations of silicate ($Si(OH)_4$),

water samples were subsequently filtered through a 0.45-μm acetate cellulose membrane and stored at 4 °C until analysis. For the determination of dissolved inorganic nitrogen (i.e., $DIN = NO_3^- + NO_2^- + NH_4^+$) and phosphate concentrations (PO_4^{3-}), water samples were immediately stored at − 20 °C. The samples were analyzed within 1 month after field collection with an auto-analyzer (Technicon III) following standard protocols (Aminot and Kérouel 2007; Hydes et al. 2010). The limits of quantification were 0.2 μM for silicate, 0.1 μM for nitrate, 0.02 μM for nitrite, 0.04 μM for phosphate, and 0.1 μM for ammonia.

Suspended Particulate Matter

SPM was filtered following the method of Aminot and Chaussepied (1983). The concentration of SPM in each sample was obtained after filtration (filtrated volume ranging from 0.1 to 1 L depending on turbidity) and drying for 24 h at 50 °C on pre-weighed calcined (i.e., 6 h; 450 °C) GF/F filters (47 mm, 0.7 μm). Filters were rinsed with distilled water to remove any remaining salt. This strategy ensured a precision of 0.0001 g L^{-1} for the lowest SPM concentrations (Verney et al. 2009).

Biomass Measurements

Phytoplankton biomass was assessed based on chlorophyll a (chl$a$) concentrations. Samples (30–500 ml) were filtered in
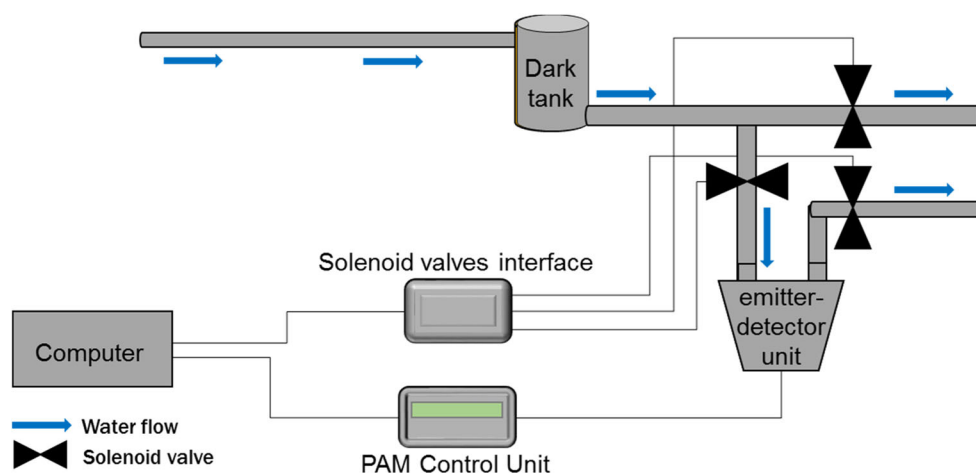
Fig. 2 Schematic diagram of the sampling strategy for high-frequency measurement of photosynthetic parameters. A pump-connected pipe was immersed to sub-surface (1 m) from the ship deck, and water was introduced periodically (5-min interval) to the insulated dark tank for dark adaptation of photosystem, and then automatically flowed into the PAM flow through chamber for measurement of photosynthetic parameters. The water flow was controlled by solenoid valve automatically activated using a homemade software. The device was controlled semi-automatically as it was necessary to adjust the gains and performed blank between some samples according to chl*a* concentration variability. Therefore, an operator was necessary to control the device

triplicate through glass-fiber filters (Whatman, GF/F, 47 mm, 0.7 μm) and immediately frozen (− 20 °C) until analysis. In the laboratory, pigments were extracted in 10 mL of 90% (*v/v*) acetone for 12 h in the dark at 4 °C. After centrifugation at 2000*g* for 10 min at 4 °C, the concentration of chl*a* were measured on extracts according to the fluorometric method of Lorenzen (1966) using a Turner Trilogy fluorometer (Turner Designs, Sunnyvale, California, USA).

Estimation of Primary Production

PAM Fluorometry

For the high-frequency estimation of primary production, the maximum quantum yield of PSII (F_V:F_M) was measured at 5-min intervals using the flow through (FT) version of the WATER PAM (Waltz, Effeltrich, Germany) (Schreiber et al. 1986). Sub-surface water was collected through a pipe leading to a thermally insulated dark reserve that maintained the sample at the in situ temperature (Fig. 2). After 5 min of dark acclimation, which was sufficient for the oxidation of the Quinone A (Q_A) pool in this highly turbid environment, a sub-sample was automatically transferred into the measuring chamber. The sample was excited by a weak blue light (1 μmol m^{-2} s^{-1}, 470 nm, frequency 0.6 kHz) to record the minimum fluorescence (F_0). Maximum fluorescence (F_M) was obtained during a saturating light pulse (0.6 s, 1700 μmol m^{-2} s^{-1}, 470 nm) allowing all the Q_A pool to be reduced. F_V:F_M was calculated according to the following equation (Genty et al. 1989):

$$\frac{F_V}{F_M} = \frac{(F_M - F_0)}{F_M} \tag{1}$$

Consecutively, samples were exposed to nine irradiances (E) from 0 to 469 μmol photon m^{-2} s^{-1} from January to July and from 0 to 1541 from August to December for 30 s for each light step. Steady state fluorescence (F_S) and maximum fluorescence (F_M') were measured. The effective quantum yield of PSII for each irradiance was determined as follows (Genty et al. 1989):

$$\frac{\Delta F}{F_M'} = \frac{(F_M' - F_S)}{F_M'} \tag{2}$$

The relative electron transport rate (rETR, rel.unit) was calculated for each irradiance. rETR is a measure of the rate of linear electron transport through PSII, which is correlated with the overall photosynthetic performance of the phytoplankton (Juneau and Harrison 2005):

$$rETR(E) = \frac{\Delta F}{F_M'} \times E \tag{3}$$

At each site, a sample of both sub-surface water and water at the WSI were taken and dark adapted for 5 min. A sub-sample was inserted into the measuring chamber of the cuvette version of the WATER PAM (Waltz, Effeltrich, Germany) and rETR versus E curves were performed as described above.

Another dark-adapted sub-sample was placed in a multi-color PAM (Waltz, Effeltrich, Germany) for estimation of the wavelength-dependent functional cross section of PSII (σ_{PSII}; expressed in m^2) derived from the initial rise of fluorescence yield upon onset of saturating light intensity ($\lambda = 440$ nm), which directly reflects the rate at which PSII centers are closed. This cross section may be visualized as the effective area of a PSII unit, exposed to a beam of photons, with the size of this area varying with the pigment composition and the

color of the incident light (Schreiber et al. 2012). Calculation of $\sigma_{PSII400}$ by the multi-color PAM software is based on the following equation (Klughammer and Schreiber 2015):

$$\sigma_{PSII_{440}} = \frac{PAR(II)}{L \times PAR} \tag{4}$$

where L is Avogadro's constant, PAR is the quantum flux density of the light driving the O-I_1 rise expressed in µmol quanta/(m^2 s^{-1}), and PAR(II) is the rate of quantum absorption in PS II expressed in units of quanta/(PSII s^{-1}). As explained by Schreiber et al. (2012), this definition of $\sigma_{PSII400}$ relates to the functional cross section of PSII for the specific conditions under which the O-I_1 rise measurement was carried out. $\sigma_{PSII400}$ specifically applies for the reference state of a dark-adapted sample with open PSII reaction centers and oxidized PQ pool. It is not identical to the functional PSII cross section defined by Kolber et al. (1998) and, hence, can be modulated by changes in the PQ-redox state and various types of non-photochemical quenching.

Consequently, based on PAR(II) which can be expressed from Eq. 4 as PAR(II) = $\sigma_{PSII400} \times L \times PAR$, also a wavelength- and sample-dependent ETR(II) can be defined:

$$ETR(II) = PAR(II) \times \frac{\Delta F : F_M{}'}{F_V : F_M} \tag{5}$$

After application of the mechanistic model of Eilers and Peeters (1988) to estimate rETR$_{max}$ from rETR/E curves previously performed, and according to Eqs. 4 and 5, as Schreiber et al. (2012), the maximum ETR(II)$_{max}$ was calculated. Firstly, ETR(II)$_{max}$ was expressed in electron (PSII s^{-1})$^{-1}$ using Eq. 6 and secondly ETR(II)$_{max}$ was expressed in mmol electron mg chl^{-1} h^{-1} according to Eq. 7:

$$[ETR(II)_{max}] = \frac{rETRmax \times \sigma_{PSII} \times L}{F_V : F_M} \tag{6}$$

$$ETR(II)_{max} = \frac{[ETR(II)_{max}] \times [PSII] \times 36.10^6}{[chla] \times L} \tag{7}$$

within Eq. 6, F_V:F_M and rETR$_{max}$ (knowing that rETR = PAR $\times \Delta F$:$F_M{}'$) calculated above, L the Avogadro's constant in mol^{-1} and σ_{PSII} in m^2. Then, in Eq. 7, [ETR(II)$_{max}$] calculated from Eq. 6 and expressed in electron (PSII s^{-1})$^{-1}$, 36 × 10^6 the factor to change units from seconds to hours and from mol to mmol, [chla] the chlorophyll concentration expressed in mg ml^{-1} and [PSII] the concentration of PSII reaction centers in PSII ml^{-1} obtained as follows:

$$[PSII] = \frac{[chl\ a] \times L}{900 \times 1000} \tag{8}$$

where [chla] represents the overall chla content in the sample expressed in g ml^{-1} assuming as Schreiber et al. (2012) a molecular weight of 900 g mol^{-1} per chl, an Avogadro's

constant of 6.022×10^{23} molecules per mol and 1000 molecules of chla per PSII unit.

^{13}C Incorporation

A photosynthetron (modified by Babin et al. (1994)) was used to incubate ^{13}C on the samples taken at sites 2, 4, 6, and 8. A U-shaped dimmable fluorescent tube (OSRAM, DULUX L, 2G11, 55 W/12–950, LUMILUX DE LUXE, daylight) produced the light, and the temperature in the photosynthetron was maintained at the in situ temperature by a seawater circuit equipped with a water chiller (AQUAVIE ICE 400). A total of 1100 ml of seawater was inoculated with NaH^{13}CO$_3$ (98 atom %, Sigma) corresponding to an enrichment of about 15% of the dissolved inorganic carbon already present in the seawater. The inoculated seawater was shared among 16 culture flasks (62 ml) placed in the photosynthetron. Light intensity was measured in each flask using a micro-spherical quantum sensor (US-SQS; Walz) connected to a LI-COR 1400 data logger. One of the flasks was kept in the dark to estimate incorporation of non-photosynthetic inorganic carbon. The light values ranged between 0 and 1550 µmol photons m^{-2} s^{-1}.

After 3 h of incubation, each flask was filtered onto 25 mm pre-combusted (450 °C, 12 h) GF/F filters and stored at − 20 °C until analysis. To remove carbonates, filters were exposed to fuming HCl for 4 h and then dried at 50 °C for 12 h. The concentration of particulate organic carbon (POC) and the isotopic ratio of ^{13}C to ^{12}C were determined using an elemental analyzer (EA 3000, Eurovector) combined with a mass spectrophotometer (IsoPrime, Elementar). As already discussed in previous studies (Lawrenz et al. 2013; Milligan et al. 2014; Hancke et al. 2015) concerning GPP (gross primary production) and NPP (net primary production) estimations, it is still debated for ^{13}C or ^{14}C incubation of few hours. The carbon fixation rate (P$_{obs}$) was calculated according to Hama et al. (1983). The value for incorporation in the dark was subtracted from all data, and P$_{obs}$ is expressed in mmol C L^{-1} h^{-1}.

P vs. E Curves

Each ETR(II) and P$_{obs}$ series were plotted against light (E). To estimate photosynthetic parameters, the mechanistic model of Eilers and Peeters (1988) was applied to these plots using SigmaPlot 12.0 (Systat Software):

$$X(E) = \frac{E}{(aE^2 + bE + c)} \tag{9}$$

where X represents either ETR(II) or P$_{obs}$. Thereby, the maximum photosynthetic capacity (ETR(II)$_{max}$ or P$_{max}$) and the

low maximum light utilization efficiency (α) were calculated as follows:

$$X_{max} = \frac{1}{\left(b + 2\sqrt{ac}\right)} \tag{10}$$

$$\alpha = \frac{1}{c} \tag{11}$$

Estimation of the Annual Primary Production

Carbon incorporation (P_{max}) was plotted against $ETR(II)_{max}$ to investigate the relationship between the two parameters. The electron requirement for C fixation ($\varphi_{e,C}$) dynamics characterized by the slopes of the relationships (Napoléon et al. 2013b; Lawrenz et al. 2013) was also expressed. Successive multiple regressions were performed to identify the best relationship to estimate P_{max} as a function of $ETR(II)_{max}$ but also as a function of the other physical-chemical parameters (temperature, salinity, DIN, P, Si, and SPM), and this relationship was used to estimate simulated carbon incorporation P^{sim}_{max} (mg C m^{-3} h^{-1}) and α^{sim} (mg C m^{-3} h^{-1}. (µmol photon m^{-2} s^{-1})$^{-1}$). The parameter E_k was calculated as $E_k = rETR_{max}/\alpha$ and used to estimate $\alpha(II)$ from $ETR(II)_{max}$ and α^{sim} from P^{sim}_{max}.

Finally, primary production was estimated for each site for the whole study year. PPP was estimated for each hour of daylight (E) of the year and integrated with the depth of the photic zone as follows:

$$PPP\left(mgC.m^{-2}.h^{-1}\right) = \frac{n}{i} \times \int_{z_0=0.05}^{z_i=n} P^{sim}_{max}$$
$$\times \left(1 - e^{\left(-\alpha^{sim} \times \frac{E_{z_i}}{P^{sim}_{max}}\right)}\right) dz \tag{12}$$

where z is the depth, i the number of replicates, and n the maximum depth of the photic zone (the limit of the photic zone was determined when 99% of the incident light was attenuated). P^{sim}_{max} (mg C m^{-3} h^{-1}) and α^{sim} (rel.unit) are the values previously calculated for each sampling month. E_{z_i} is the irradiance (µmol photon m^{-2} s^{-1}) at depth z_i calculated at 0.01 m intervals along the photic zone, which, in this study extended from 0 to 3.5 m ($i = 35$ and $n = 3.5$), using the Beer-Lambert law as follows:

$$E_{z_i} = 0.94 \times \left(E_{z_0} \times e^{-kd \times z_i}\right) \tag{13}$$

where E_{Z0} is the incident light at the surface obtained from the nearest national weather station (18 miles; 29 km), 0.94 is the percentage of light penetration into the water. k_d is the coefficient of light attenuation in the photic zone, which varied in space and over time at each site. The k_d values were calculated with the PAR attenuation observed with the depth, both measured with the SBE profiles recorded during the sampling campaigns following the equation:

$$PAR = a\, e^{-k_d \times z} \tag{14}$$

where PAR is the light (µmol photons m^{-2} s^{-1}) measured at each depth (z). The different values of k_d were estimated for each site and each month using the linear relationship found between turbidity (NTU) and the light attenuation coefficients (k_d): $k_d = 0.1107 \times$ Turbidity $+ 0.588$ ($R^2 = 0.923$). For turbidity ranging from 4.88 to 93.31, the corresponding k_d ranged from 1.13 to 10.92 mm^{-1}. P:B ratio (mg C mg chla^{-1} day^{-1}) was also estimated using these PPP estimations.

Data Analysis

Multivariate Analyses

In order to characterize the spatial and temporal variation diagram of the physical and chemical parameters, partial triadic analyses (PTA) were performed on the data set using the ADE-4 package (Chessel et al. 2004; Dray and Dufour 2007) with R software. Data were organized in sub-matrices for each site. The interstructure of the PTA consisted in comparing the structure shared between sub-matrices and in identifying sites with similar temporal structure. The second step consisted in constructing a compromise that enabled us to build a common temporal typology between matrices. The relationship between physical, chemical, biological, and photosynthetic parameters was investigated by principal component analyses (PCA) using the ADE-4 package in R software. PCA was performed of the group of sites shown by PTA to have a similar annual structure.

Univariate Analyses

In a complementary way, the linear dependence between parameters was established by linear regressions performed on R software and by calculation of Person correlation coefficient. All plots of the parameters dynamics were created using the SigmaPlot 12.0 software. The illustrative plots performed on the different parameters by taking into account the spatial and the temporal dynamics were previously smooth using the nonparametric method of local regression ("Loess"). To identify the physical-chemical parameters that significantly drive the ETR/P relationship, multiple regressions with temperature, salinity, nutrients concentrations (DIN, P, and Si), and SPM were performed using an upward step-by-step method on R software.

Results

Dynamics of Hydrological Parameters

The dynamics of the physical and chemical parameters (irradiance, river flow, temperature, salinity, nutrients, turbidity, and SPM) are characteristics for the Northern European estuaries and are therefore described in supplementary material. In order to investigate the seasonal pattern and the functioning of the estuary in a spatial context, a PTA was performed on physical and chemical parameters from sub-surface and deep waters.

Interstructure Analyses of the PTA

In the interstructure analysis of the PTA, the two first eigenvectors represent respectively 78 and 10% of total inertia of the sub-surface waters (Fig. 3a) and respectively 72 and 17% of total inertia of the bottom waters (Fig. 3d). Projection of the sites on the first axis revealed the common temporal pattern among sites (Fig. 3b, e), in agreement with the high vector correlation coefficients (RV-coefficient) calculated (Table 1). Projection of the sites on the second axis divided the sampling transect into two zones and four distinct areas (Fig. 2b) in agreement with Ward's clustering method (Fig. 3c): (i) area 1 (site 1&2) and area 2 (site 3&4) grouped in zone A (downstream); and (ii) area 3 (site 5&6) and area 4 (site 7&8) grouped in zone B (upstream). The weight values were similar for all the sites, showing that any site had a particular temporal pattern (Table 1). Thus, the Seine estuary can be divided in two zones as a function of the dynamics of the physical-chemical parameters: (i) a downstream zone (zone A) stretching from longitude 0.11 (site 1) to longitude 0.30 (site 4) and characterized by high salinity (combining the polyhaline (> 18) and mésohaline (> 5) zones), and (ii) an upstream zone (zone B) stretching from longitude 0.36 (site 5) to longitude 0.51 (site 8), characterized by lower salinity (combining the mésohaline (< 18) and oligohaline (< 5) zones) and higher turbidity.).

Compromise Analyses

In the compromise analysis of the PTA, for sub-surface waters, the two first eigenvectors represented 54 and 35% of total inertia (Fig. 4a) and for bottom parameters 63 and 29% of total inertia (Fig. 4d), providing an accurate summary of the common temporal trend among sites over the sampling year. Compromise analysis revealed a clear seasonal pattern in the physical-chemical parameters both in the sub-surface and deep waters (Fig. 4b, c, e, f). The period from January to March was characterized by high DIN and Si concentrations, related to high river flow in winter. The increase in temperature in April was followed by an increase in salinity (related to the decrease in river flow) and in surface irradiance in May. The increase in phosphate concentrations between September and October was associated with the increase in SPM concentrations and turbidity. This period was also characterized by a decrease in irradiance and temperature, and in salinity in relation with the increase in river flow.

The dynamics of the physical and chemical parameters are given in supplementary material. The highest SPM and turbidity values were recorded near the limit of salt water intrusion in the upper part of the estuary that defined the MTZ. Its position is consequently influenced at daily and seasonal scales by variations of the tide and of the river flow. Since sampling was always carried out during spring tides, the localization of the MTZ was
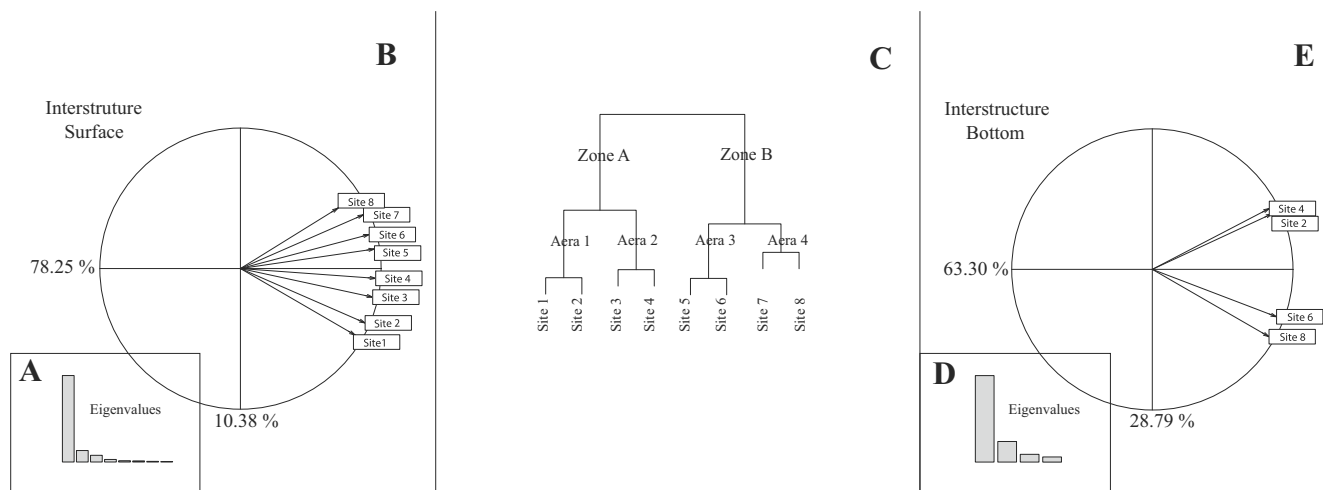

Fig. 3 Interstructure analysis of the partial triadic analysis (PTA) performed on physical-chemical parameters in the sub-surface layer. **a** Histogram of eigenvalues based on the diagonalization of the RV matrix. **b** Ordination of the sites given by the two first eigenvectors of the vector correlation matrix. **c** Tree topology obtained by Ward's clustering method. And for the bottom layer: **d** histogram of eigenvalues based on the diagonalization of the RV matrix. **e** Ordination of the sites given by the two first eigenvectors of the vector correlation matrix

Table 1 Matrix of the RV coefficients between the sub-matrix and the weight of each sub-matrix in the construction of the compromise

Sites	1	2	3	4	5	6	7	8	Weight
Surface									
1	1.00								0.33
2	0.89	1.00							0.35
3	0.82	0.90	1.00						0.38
4	0.76	0.86	0.95	1.00					0.38
5	0.69	0.78	0.86	0.90	1.00				0.38
6	0.62	0.69	0.80	0.86	0.94	1.00			0.37
7	0.55	0.61	0.72	0.81	0.89	0.92	1.00		0.35
8	0.44	0.51	0.57	0.60	0.63	0.60	0.67	1.00	0.28
Bottom									
2	1.00								0.50
4	0.76		1.00						0.49
6	0.62		0.56		1.00				0.52
8	0.50		0.51		0.80		1.00		0.49

only controlled by the Seine river flow. Consequently, the MTZ was located downstream of zone B during the high-flow period and upstream during the low-flow period. Within both zones, high DIN and Si concentrations were negatively related to salinity and positively with river flow, suggesting a strong control by freshwater outputs. Indeed, in the Seine river, a large part of the DIN pool originates from agricultural and industrial activities and urban discharges along its watershed (Garnier et al. 2010), while Si is weakly influenced by human activities (Sferratore et al. 2006; Aminot and Kérouel 2007). Despite the decrease in P in the Seine River in the last few years, due to the improved waste water treatment plants and the massive introduction of detergents without phosphates, high concentrations were nevertheless measured throughout the estuary (Némery and Garnier 2007; Passy et al. 2016). In this study, P concentrations varied differently than DIN and Si in the two zones: P was positively linked with turbidity and SPM in zone A, whereas in the zone B, P concentrations were positively linked with salinity and negatively related to the Seine river flow. P is adsorbed onto suspended particles in
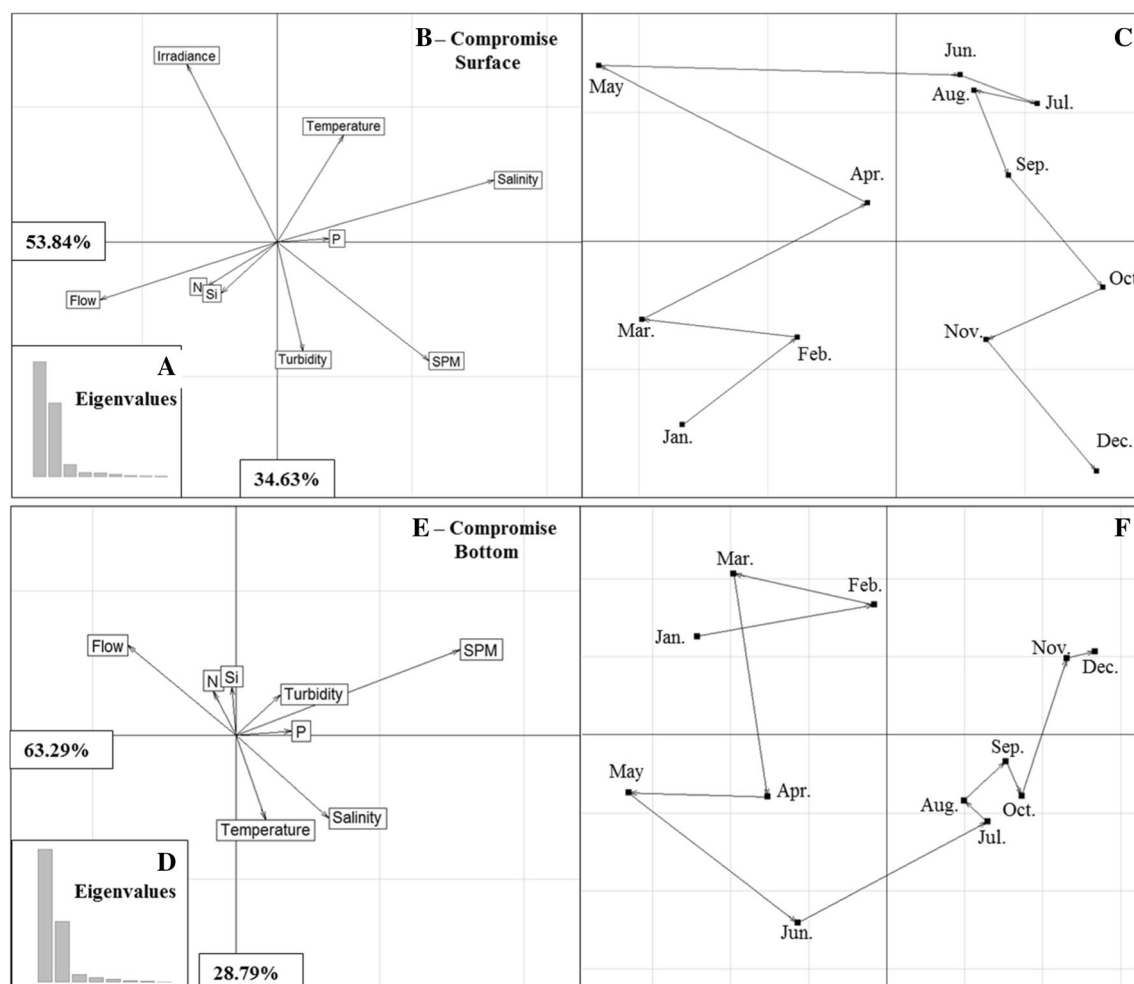

Fig. 4 Compromise analysis of the partial triadic analysis (PTA) performed on physical-chemical parameters in the sub-surface waters. Histogram of eigenvalues (**a**), projection of the variables (**b**), and the sampling dates (**c**) in the plane defined by the two first axes and for bottom waters: histogram of eigenvalues (**d**), projection of the variables (**e**), and the sampling dates (**f**) in the plane defined by the two first axes

the low-salinity and high-turbidity part of estuaries, which can be explained by non-biological buffering mechanisms (Morris et al. 1981; Sharp et al. 1982; Némery and Garnier 2007). The positive relationship with SPM and turbidity in zone A together with the negative relationship with river flow in zone B suggest the adsorption of P within the MTZ. The pool of P is then exported downstream by the SPM. The inverse relationship observed between P and river flow in zone B could be due to an accumulation of P during the low-flow periods.

Phytoplankton Biomass and Photosynthetic Parameters

The chlorophyll a concentrations ranged from 0.2 to 15.9 μg L^{-1}. In sub-surface (Fig. 5a), high concentrations of chl$a$ were recorded from May to September, and during this period, chl$a$ concentrations were increasing from upstream to downstream. The

highest phytoplankton biomass in sub-surface (15.9 μg L^{-1}) was measured at site 2 in July and the lowest (0.2 μg L^{-1}) at site 4 in January. Close to the WSI (Fig. 5b), in summer, the same gradient than in sub-surface was observed but with lower values: the highest value measured in July was 8.6 μg L^{-1} at site 2. The lowest value (0.4 μg L^{-1}) was measured in zone A during January. Surprisingly, in zone B, high chl$a$ values (> 10 μg L^{-1}, up to 21.8 μg L^{-1}) were recorded in winter.

The maximum quantum efficiency of PSII (F_V:F_M), which represents the physiological state of the cells, showed distinctive dynamics in sub-surface in comparison with the bottom waters. In sub-surface (Fig. 5c), F_V:F_M were high in winter and spring with the highest value (0.67) measured in March at site 1. In contrast, the lowest value (< 0.01) was measured during summer (July) at site 8. In the upstream part of the estuary (Zone B), F_V:F_M were low with values remaining frequently below 0.20. Close to
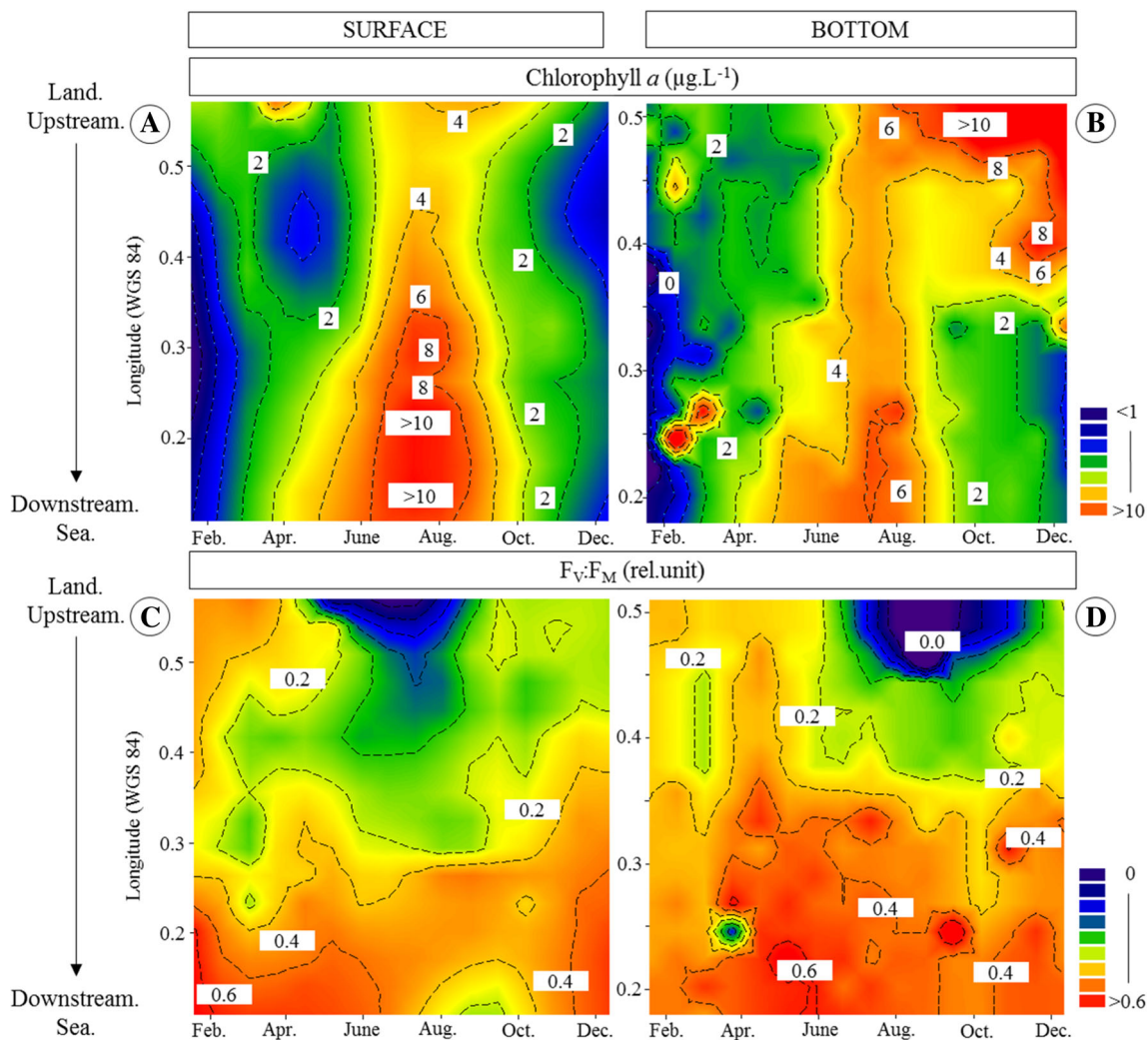

Fig. 5 Variations in biomass (chl$a$ concentration; μg L^{-1}) and the maximum quantum efficiency of PSII (F_V:F_M; rel.unit) representing the physiological state of the cells in the Seine estuary from January to December, 2015. The sub-surface layer (1 m) is shown in the left panel and the bottom layer (1 m above the WSI) in the right panel

the WSI (Fig. 5d), the highest value (0.64) was measured at site 2 in May and the lowest (< 0.01) at site 8 in August. F_V:F_M ratios close to the WSI showed high values in Zone A, with an average of 0.41 during the year, while in Zone B, the F_V:F_M ratios remained low with an average of 0.16 during the studied period.

The high values of chl$a$ observed close to the WSI in winter were associated to very low values of F_V:F_M which indicates that this biomass is rather freshwater chlorophyll detrital matter than living phytoplankton.

The maximum light utilization efficiency (α(II); mmol electron mg chla^{-1} h^{-1}.(μmol photon m^{-2} s^{-1})$^{-1}$), were highly variable in space and time (Fig. 6). In January, low values (i.e., < 0.008 mmol electron mg chla^{-1} h^{-1}.(μmol photon m^{-2} s^{-1})$^{-1}$) were recorded throughout the salinity gradient and within the MTZ area from January to March and from August to December. In May at longitude 0.4, a zone with values < 0.008 was also recorded. Higher α(II) were observed during the rest of the year, with the highest values (> 0.012 mmol electron mg chla^{-1} h^{-1} (μmol photon m^{-2} s^{-1})$^{-1}$) measured in the polyhaline zone (longitude < 0.2) between February and October. From February to December, a spatial gradient appeared to mirror the salinity gradient with decreasing values from downstream to upstream.

The dynamics of ETR(II)$_{max}$ (Fig. 7) showed low values (i.e., < 2 mmol electron mg chl^{-1} h^{-1}) throughout the salinity gradient in winter (January and February). ETR(II)$_{max}$ started to increase from March, firstly in the downstream part of the estuary and throughout the salinity gradient afterwards. The highest values were recorded from June to October throughout the salinity gradient. ETR(II)$_{max}$ were particularly high in the polyhaline zone with a maximum value of 10.8 mmol electron mg chl^{-1} h^{-1}

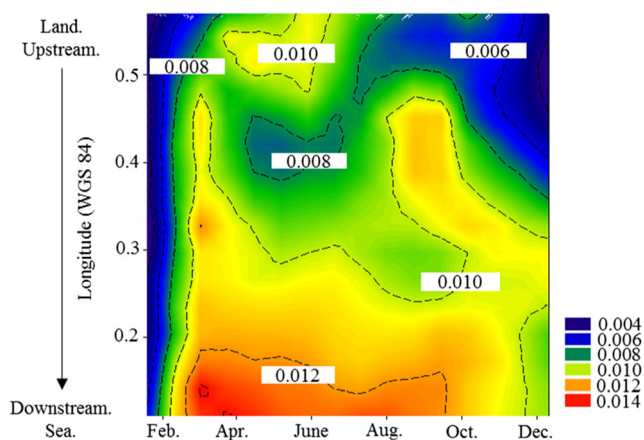**Fig. 7** Variations in the maximum electron transport rate (ETR(II)$_{max}$; mmol electron mg chl^{-1} h^{-1}) in the Seine estuary from January to December, 2015. The ETR(II)$_{max}$ was measured at 5-min intervals in the sub-surface layer of water all along the sampling transect at monthly intervals

at site 2 in June. During this period of high ETR(II)$_{max}$, values gradually increased from upstream to downstream.

Estimation of $\varphi_{e,C}$ and of Primary Production

The combined PAM and carbon incorporation method was used to investigate the relationship between P$_{max}$ et ETR(II)$_{max}$ measurements (Napoléon and Claquin 2012; Lawrenz et al. 2013), and P$_{max}$ values were plotted against the ETR(II)$_{max}$ values (Fig. 8).

The electron requirement for C fixation ($\varphi_{e,C}$; mol electron mol C^{-1}), defined by the slope of the relationship between P and ETR, varied spatially and temporally ranging from 1.6 to 25 mol electron mol C^{-1} (Fig. 9). A marked seasonal pattern was observed, characterized by high values (> 15 mol electron mol C^{-1}) throughout the salinity gradient in January and only in the downstream part in February and March (e.g., 25 mol electron mol C^{-1} at site 2 in March). High values were also estimated upstream during the summer (22.2 mol electron mol C^{-1} at site 8 in July). $\varphi_{e,C}$ values < 4 mol electron mol C^{-1} were recorded twice: 1.6 mol electron mol C^{-1} at site 6 in May and 1.9 mol electron mol C^{-1} at site 8 in December. The mean $\varphi_{e,C}$ value was 8 ± 5 mol electron mol C^{-1}.

To identify the physical-chemical parameters that drive this relationship between P and ETR(II), multiple regressions with temperature, salinity, nutrients concentrations (DIN, P, and Si), and SPM were performed using an upward step-by-step method. A significant negative coefficient with DIN concentrations and a significant positive coefficient with temperature were observed. These two parameters were used to estimate

Fig. 6 Variations in the low maximum light utilization efficiency (α(II); mmol electron mg chl$a$ h^{-1} .(μmol photon m^{-2} s^{-1})$^{-1}$) in the Seine estuary from January to December, 2015. This parameter was measured at high frequency in the sub-surface layer of water all along the sampling transect at monthly intervals
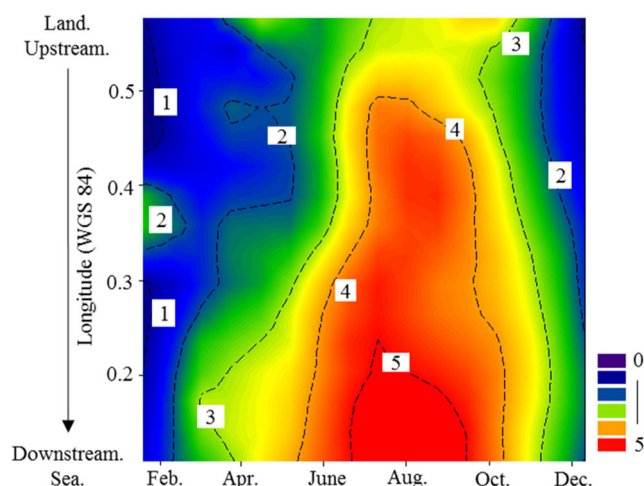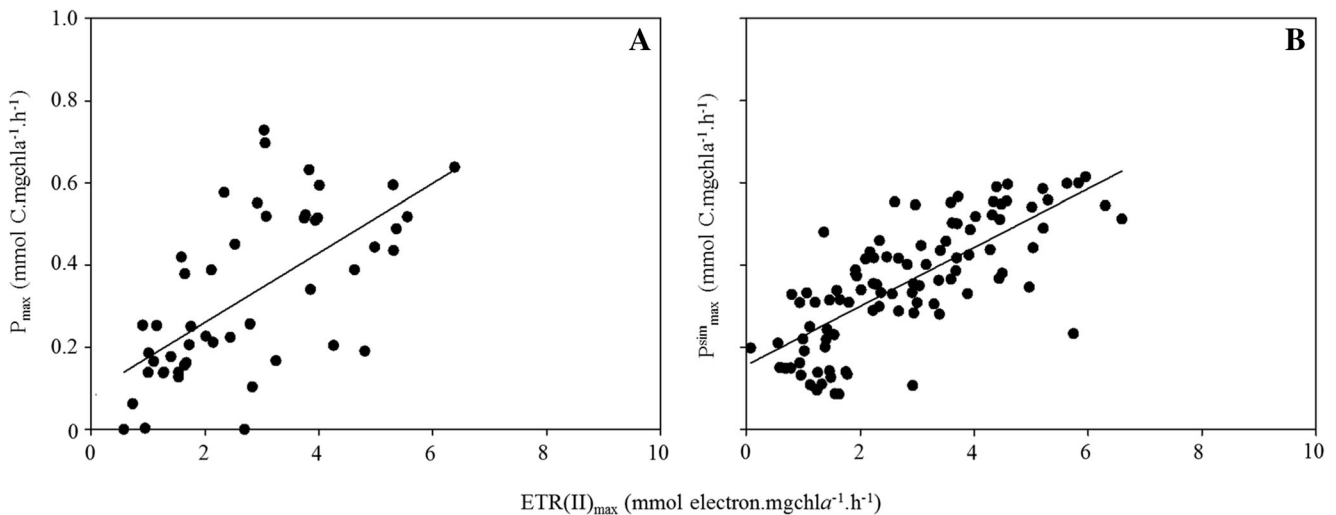
Fig. 8 a Relationship between ETR(II)$_{max}$ (mmol electron mg chl^{-1} h^{-1}) and P$_{max}$ (mmol c mg chl^{-1} h^{-1}) measured in the Seine estuary from January to December, 2015. b Relationship between ETR(II)$_{max}$ (mmol electron mg chl^{-1} h^{-1}) and P$^{sim}_{max}$ (mmol c mg chl^{-1} h^{-1}) calculated using the following equation: P$^{sim}_{max}$ = 0.43−1.19.10^{-2} × ETR (II)$_{max}$−9.75.10^{-4} × [DIN] + 1.29.10^{-2} × Temperature (Eq. 15 in the text)

the P$_{max}$ dynamics ($p < 0.0001$; $R^2 = 0.59$) by using ETR(II)$_{max}$ according to the following equation:

$$P^{sim}_{max} = 0.43 - 1.19.10^{-2} \times ETR(II)_{max} - 9.75.10^{-4}$$
$$\times [DIN] + 1.29.10^{-2} \times Temperature \quad (15)$$

A carbon incorporation at high frequency (P$^{sim}_{max}$) and a maximum light utilization efficiency (α_{sim} = ratio Ek/P$^{sim}_{max}$) were then estimated for each value of ETR(II)$_{max}$ (Fig. 8). For each site, these values of P$^{sim}_{max}$ and α_{sim} were used to estimate PPP at each hour of daylight (E) throughout the year by using a depth integrated equation of light penetration as a function of turbidity (Eqs. 10 and 11).

The dynamics of annual PPP showed high variability that differed at each time scale: at the hourly scale, values reached 110.4 mg C m^{-2} h^{-1}, at the daily scale, values reached 1.2 g C m^{-2} day^{-1}, and at the monthly scale values reached 26.1 g C m^{-2} month^{-1} at site 2 in July (Table 2; Fig. 10). When considering all the sites, the highest PPP were observed in July, with a mean of 13.2 g C m^{-2} m^{-1}. Annual PPP was minimum at site 6 with a value of 17.3 g C m^{-2} year^{-1} and maximum at site 2 with a value of 81.5 g C m^{-2} year^{-1}.

A representative area (in km^2) was attributed to each site as a function of the water cover at high tide. Primary production values are expressed in t C year^{-1} for each of these areas. Results revealed the prime role played by the mouth of the estuary (represented by site 1). Despite the better production capacity per m^2 at site 2, the area represented by site 1 (44.38 km^2) led a higher carbon production with 3200 t C year^{-1}. When primary production was weighted as a function of the surface area of each site, the mean value for the annual PPP in the Seine estuary in 2015 was 64.75 g C m^{-2} year^{-1}.

The measured P:B ratio in sub-surface varied between 1 and 7.4 mg C mg chla^{-1} h^{-1} with a mean value of 4.2 mg C mg chla^{-1} h^{-1}. The spatial gradient of P:B ratio (mg C mg chla^{-1} day^{-1}) integrated along the photic layer showed higher values downstream than upstream (Fig. 10). The maximum P:B ratio (19.6 mg C mg chla^{-1} day^{-1}) was recorded in the mouth of the estuary in spring. In summer, the highest values were observed in the mesohaline part of the estuary.

Principal Component Analyses

Two PCA were performed to investigate the relationship between physical-chemical and biological parameters in the sub-surface waters (Fig. 11a, b) and bottom waters (Fig. 11c, d), the data sets representing the two zones defined by the PTA
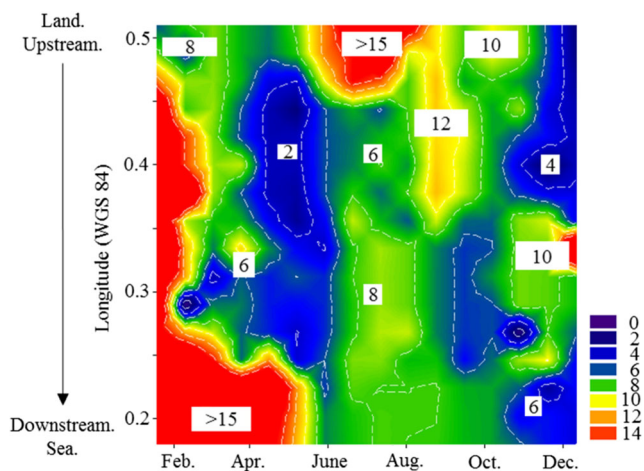

Fig. 9 Dynamics of electron requirements for C fixation ($\varphi_{e,C}$) in the Seine estuary from January to December, 2015

Table 2 Estimation of phytoplankton primary production (g C m^{-2} m^{-1}) for each month (from January to December) and at each site (from 1 to 8). The minimum and maximum daily PPP (g C m^{-2} day^{-1}) are given and an annual PPP (in g C m^{-2} year^{-1} and in t C year^{-1}) was calculated for each site (bottom row). A mean PPP (g C m^{-2} m^{-1}) was calculated for each month (last column on the right) and on average for the estuary (last cell on the bottom right)

Site	1	2	3	4	5	6	7	8	Mean (g C m^{-2})
January	0.27	0.22	0.11	0.05	0.01	0.03	0.02	0.09	0.10
February	1.53	1.06	0.72	0.38	0.37	0.37	0.44	0.27	0.64
March	1.39	0.83	0.43	0.29	0.30	0.32	0.35	0.37	0.54
April	7.47	5.61	2.35	2.09	0.87	0.33	0.15	0.88	2.47
May	15.14	9.78	4.65	2.79	1.87	1.89	3.24	4.43	5.47
June	10.72	10.82	8.10	9.18	4.87	5.38	2.65	3.66	6.92
July	18.95	26.09	21.64	17.43	11.00	4.93	2.76	2.43	13.15
August	8.58	19.87	7.56	8.34	8.76	2.05	6.66	3.06	8.11
September	3.33	3.46	3.01	2.66	1.12	1.12	0.93	1.14	2.10
October	2.57	2.60	1.01	1.49	1.60	0.70	0.36	1.32	1.45
November	1.99	0.87	0.82	0.84	0.21	0.05	0.01	0.89	0.71
December	0.19	0.32	0.28	0.15	0.16	0.11	0.06	0.02	0.16
Max PPP (g C m^{-2} day^{-1})	0.83	1.18	0.94	0.77	0.49	0.23	0.28	0.17	–
Min PPP (g C m^{-2} day^{-1})	2^{-3}	3^{-3}	2^{-3}	9^{-4}	2^{-4}	5^{-4}	9^{-5}	2^{-4}	–
Annual PPP (g C m^{-2} year^{-1})	72.13	81.53	50.68	45.68	31.16	17.26	17.62	18.54	–
Surface (km^{-2})	44.38	23.07	9.81	4.27	3.79	2.61	2.26	2.96	–
Annual PPP (t C year^{-1})	3200	1881.3	497.15	195.26	118.15	45.09	39.84	54.92	64.75 g C m^{-2} year^{-1}

performed on physical-chemical parameters (Fig. 3). In zone A and zone B, the two first axes of the PCAs explained respectively 72 and 71.% of the total inertia for sub-surface waters, and for both, 76% of the total inertia for bottom waters. Analyses were thus based on these two axes.

For both zones (A and B), the parameters that contributed the most to axis 1 were salinity and temperature in one direction, and Si, DIN, and flow in the other direction for sub-surface waters. Regarding the second axis, the parameters that contributed the most were irradiance in one direction and turbidity and the SPM concentrations in the other direction. Despite their low contribution, chl*a* concentrations were positively linked with temperature in both zones. Daily phytoplankton primary production (dPPP) and P:B ratio were positively linked with irradiance and temperature and negatively linked with turbidity. The P concentration varied between the
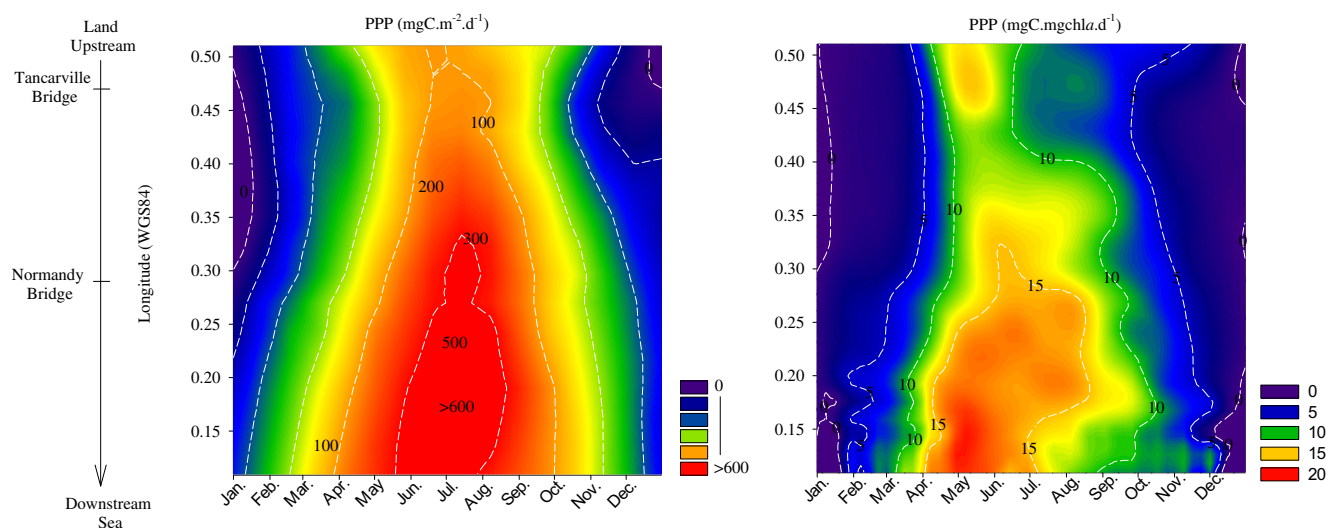

Fig. 10 Dynamics of daily phytoplankton primary production (left; mg C m^{-2} day^{-1}) and P:B ratio (right; mg C mg chl*a*$^{-1}$ day^{-1}) along the Seine estuary from "Le Havre" (longitude 0.09) to "Tancarville" (longitude 0.51) in 2015. PP was estimated as a function of hourly irradiance and integrated over depth
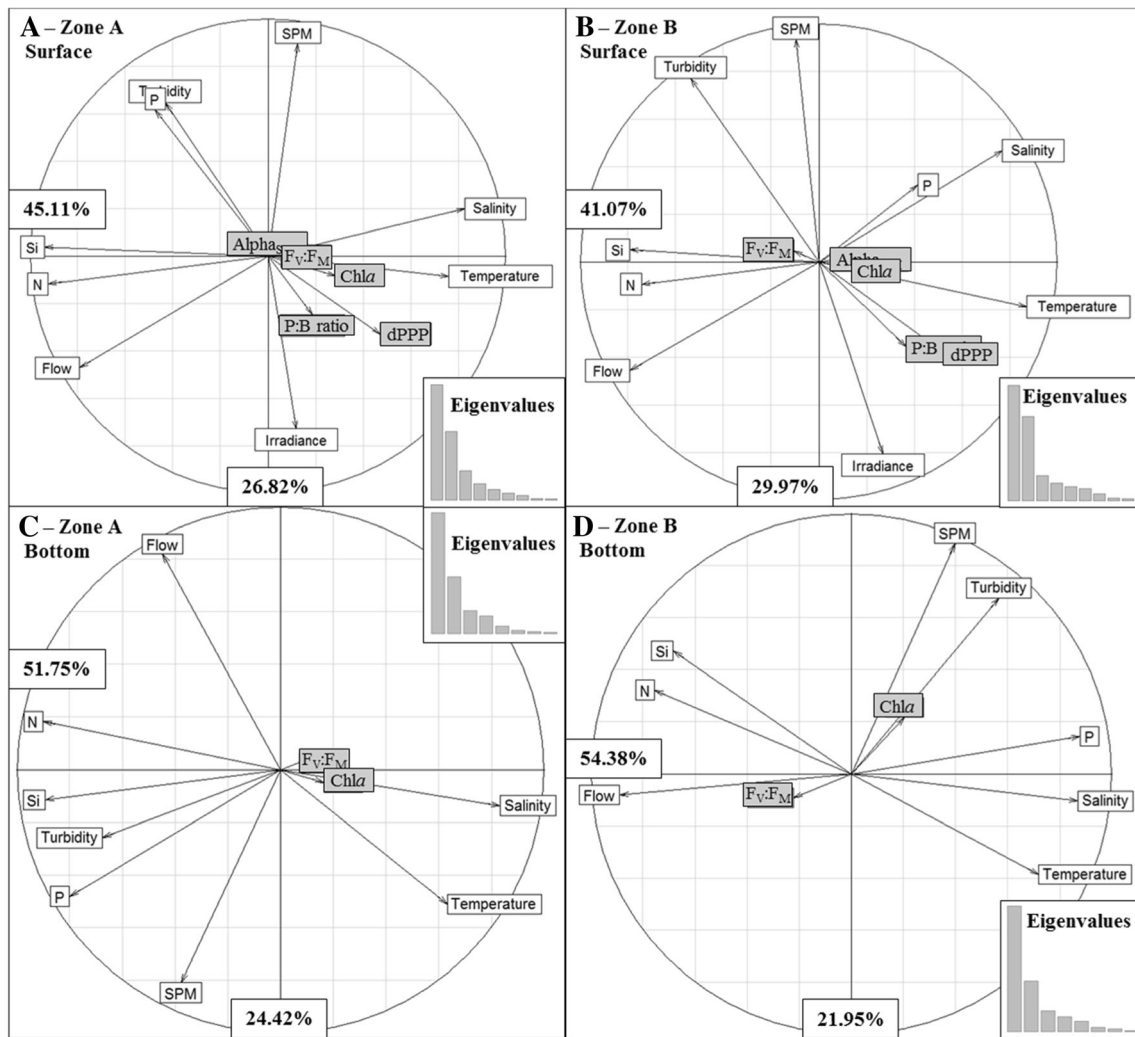
Fig. 11 Principal component analysis factor loading plot in the plane defined by the two axes for sub-surface waters. **a** Zone A (sites 1 to 4) and **b** zone B (sites 5 to 8) and for bottom waters with (**d**) zone A and (**e**) zone B. White labels show active variables and gray labels illustrative variables

two zones and was related to turbidity in zone A and to salinity in zone B. The variations in F_V:F_M and α_{sim} were poorly explained by the physical-chemical parameters tested in both PCA.

In the bottom waters in zone A, the parameters that contributed the most to axis 1 were salinity and temperature in one direction and Si and DIN in the other direction. The parameters that contributed the most to axis 2 were the river flow in one direction, and SPM concentrations in the other. Despite their limited contributions, chl$a$ concentrations and F_V:F_M were positively linked with salinity. In zone B, the parameters that contributed the most to axis 1 were salinity and P concentration in one direction and the river flow in the other direction. The parameters that contributed most to axis 2 were SPM and turbidity in one direction and temperature in the other direction. The biological parameters contributed more than in

zone A, and chl$a$ concentrations were positively linked with turbidity and F_V:F_M positively linked with flow.

Discussion

Phytoplankton Biomass and the Dynamics of Photosynthetic Parameters

Nutrient concentrations were very high throughout the year and were not limiting for phytoplankton growth. Despite a negative relationship between chl$a$ and the concentrations of nutrients (DIN and Si), the role of phytoplankton consumption on nutrient dynamics may have been weak in regard to the importance of nutrients fluxes which are mostly controlled by hydrodynamics (Kromkamp and Peene 2005). Classically, the dynamics

of chl*a* in nutrient-rich estuaries is mostly controlled by light availability, which varies with incident solar irradiance in the photic layers modulated by turbidity. The spatial dynamics of chl*a* can be explained by the higher light availability downstream and osmotic stress in the most upstream part of the estuary which can lead to growth limitation and cell lysis (Lionard et al. 2005; Servais and Garnier 2006; Hernando et al. 2015). This stress could be confirmed by the low annual values of F_V:F_M ratios (< 0.2) observed upstream. However, the presence of cyanobacteria in this part of the estuary (data not shown) could also explain the low level of F_V:F_M ratios. F_V:F_M ratios of cyanobacteria are known to be poorly estimated by PAM methods because of the contribution of phycobilisomes auto-fluorescence to F_0 background, and the PSII:PSI ratio is small in cyanobacteria as opposite to diatoms for instance (Campbell et al. 1998; Masojidek et al. 2001; Macintyre et al. 2002; Suggett et al. 2004; Johnsen and Sakshaug 2007). The slightly higher F_V:F_M ratios observed from January to April could also be attributed to freshwater species adapted to low salinity, low temperature, and high turbidity as reported by in the Chesapeake bay. In zone A (downstream part), F_V:F_M ratios in sub-surface waters were higher in winter (> 0.4) than in summer (< 0.4) and inversely related to the concentrations of chl*a*. The successive stress undergone in this zone could have led to a reduction in F_V:F_M values especially with the high level of irradiance in summer. These reductions of F_V:F_M can be due to photoprotection mechanisms or to alteration of PSII. As widely described, high irradiance may lead to a reduction of F_V:F_M in sub-surface waters (Holm-Hansen et al. 2000; Shelly et al. 2003) due to the activation of short-term photoprotection mechanisms, such as xanthophyll cycling, which increases non-photochemical quenching to protect cells against high levels of irradiance (Dubinsky and Stambler 2009; Goss and Jakob 2010). Moreover, the sub-surface layer can be defined as a fluctuating light environment caused by longitudinal and vertical mixing. In this type of environment, Alderkamp et al. (2010) have shown that phytoplankton cells need to balance more rapidly their photosynthetic machinery to maximize photoprotection at high irradiance and photosynthetic efficiency at low irradiance. Due to the turbidity level in estuary, acclimation to low light is principally require which induces a reduction in photo-protective pigment content. This reduction could lead to potential damage of photosystems when cells are exposed to high light on surface during summer (Alderkamp et al. 2010). Despite the low values of F_V:F_M in summer in the downstream part, high values of α and ETR(II)$_{max}$ were measured allowing phytoplankton growth and high chl*a* concentration. This discrepancy between α, ETR(II)$_{max}$, and F_V:F_M levels can be due to

state transition mechanisms of cyanobacteria as previously described. These patterns were also observed upstream of the MTZ in the very low-salinity zone. Despite low chl*a* concentrations, the high photosynthetic values revealed a non-negligible capacity of the freshwater phytoplankton to contribute to photosynthesis in the estuary.

Regarding, the WSI values, high F_V:F_M ratios was not expected because of the high level of detritic matter in this water layer. This result suggests that a large part of the phytoplankton biomass close to the WSI was composed of healthy cells.

Carbon and ETR Relationship

The relation between ETR and carbon fixation was used to estimate carbon incorporation at high spatial frequency. The dynamics of the $\varphi_{e,C}$ showed strong temporal and spatial variability ranging between 1.56 and 24.98 mol electron mol C^{-1} with a mean value of 7.95 ± 4.94 mol electron mol C^{-1} over the course of the sampling year. Moreover, no spectral correction was performed in this study, and our values were therefore overestimated by at least a factor of 1.5 or 2 (Lawrenz et al. 2013; Hancke et al. 2015). However, because no measurement of light spectrum was performed during this study, the choice was made to keep not corrected values to avoid arbitrary corrections using constant from literature.

Under optimal growth conditions, the value of $\varphi_{e,C}$ is comprised between 4 and 6 mol. The $\varphi_{e,C}$ values lower than 4 mol electron mol C^{-1} appear to be physically impossible and could be due to methodological, calculation errors (Lawrenz et al. 2013) or particular metabolic pathway (Bailleul et al. 2015). Indeed, values lower than 4 mol electron mol C^{-1} can be attenuated to an additional source of energy used in carbon fixation. It was recently shown that diatoms are able to optimize their photosynthesis through the exchange of energy between plastids and mitochondria (Bailleul et al. 2015). Indeed, when the ATP:NADPH ratio generated by a linear electron flow is insufficient to fuel CO_2 imports into the plastid and assimilation by the Calvin cycle, diatoms are able to produce additional ATP via alternative pathways, particularly through extensive energy exchanges between plastids and mitochondria. This process could explain values of $\varphi_{e,C} < 4$ mol electron mol C^{-1}. Moreover, as mentioned above, carbon incorporation during few hours provide an estimate between NPP and GPP, which entails a variability of $\varphi_{e,C}$ values (Lawrenz et al. 2013; Hancke et al. 2015) which need to be deeply studied (Milligan et al. 2014).

In this study, the average values of $\varphi_{e,C}$ were lower than those observed in previous studies (Kaiblinger and Dokulil 2006; Napoléon et al. 2013b) despite high environmental pressures. Environmental variations are the primary source of variations in electron transport and carbon fixation which can induce high values of $\varphi_{e,C}$ such as temperature (Morris

and Kromkamp 2003), nutrient limitations (Babin et al. 1996; Napoléon et al. 2013b; Lawrenz et al. 2013; Schuback et al. 2015), or light stress (Napoléon and Claquin 2012; Zhu et al. 2016). The phytoplankton community assemblage can also influence the $\varphi_{e,C}$ values; however, this factor was not considered in the present study but will be investigated in a future work. We assume that the average value of 8 mol electrons mol C^{-1} estimated in this study could be explained by the high nutrient level recorded in the estuary over the year. Indeed, Napoléon et al. (2013b) observed a large increase of the $\varphi_{e,C}$ under nutrient limitation, up to 125 mol electron mol C^{-1}; therefore, nutrient limitation seems to largely control the ETR/C relationship. Thus, in optimal nutrient conditions, even in stressful ecosystem as an estuary, the photosynthetic apparatus appears to be able to cope with environmental variations with ease.

Regarding metabolic regulation, the $\varphi_{e,C}$ values are due to alternative electron flow pathways (AEF) between PSII and C fixation which therefore influence the ETR(II)$_{max}$/P$_{max}$ relationship. Such AEF (i.e., Mehler reaction, electron flow around PSI or/and PSII, photorespiration) modulate the ATP:NADPH ratio as a function of the metabolic demand to optimize photosynthetic performance and growth (Endo and Asada 2002; Nogales et al. 2011; Johnson and Alric 2013). Thus, the more AEF is important in comparison to LEF (linear electron flow), the more $\varphi_{e,C}$ is high and will potentially bias the estimation of carbon incorporation using the ETR(II)$_{max}$ measurements.

In this context, it is still important to investigate the variation in the ETR(II)$_{max}$/P$_{max}$ relationship (i.e., $\varphi_{e,C}$) as a function of environmental parameters. In our study, a statistic relationship was determined considering the temperature and the DIN as significant environmental parameters. This was in agreement with previous studies that have explored such as statistical relationships between ETR and C fixation which underlined the importance of temperature, nutrients, and light (Napoléon and Claquin 2012; Lawrenz et al. 2013). However, the influence rate of each parameter differs from a system to another, and it still necessary to investigate the contribution of each environmental variable in different studied area.

Phytoplankton Primary Production Along the Seine Estuary

Estimated daily carbon production in the Seine estuary reached 1.18 g C m^{-2} day^{-1} in summer. Logically, primary production was higher in summer when river flow and turbidity are lower and when temperature and irradiance level are higher. These values are in agreement with some studies carried out worldwide in temperate estuaries, which reached maximum values of 4.2 g C m^{-2} day^{-1} in the Delaware (Pennock and Sharp 1986 and citations therein), 1.7 g C m^{-2} day^{-1} in the Chesapeake (Magnien et al. 1992)

in the east coast of the USA, 2.9 g C m^{-2} day^{-1} in the Schelde in Europe (van Spaendonk et al. 1993 and citations therein), 1.17 g C m^{-2} day^{-1} in the Lena in Russia (Sorokin and Sorokin 1996), and 2 g C m^{-2} day^{-1} in the Chanchiang in China (Ning et al. 1988).

In order to understand variations in photosynthetic performance in space and over time, phytoplankton P:B ratio was investigated. The P:B ratio values were in accordance with previous studies performed in the English Channel coastal systems (Jouenne et al. 2007; Pannard et al. 2008; Napoléon and Claquin 2012). In the Seine estuary, the P:B ratio showed a seasonal pattern with low values under a temperature of 10 °C and high values in spring and summer especially in zone A (Fig. 3). The weak P:B ratio in zone B could be explained by turbidity, especially from July when levels increased up to 120 NTU. During the spring bloom, induced by increasing temperature and irradiance levels (Hunter-Cevera et al. 2016), P:B ratio was higher inside the estuary in summer. Usually in coastal waters, the consumption of nutrients in spring becomes limiting in summer and results in lower P:B ratio (Napoléon et al. 2012, 2013a). In the Seine estuary, in summer, P:B ratio was higher inside the estuary than nearby coastal waters. This result pointed out an important autochthonous PPP in summer induced by the tradeoff between nutrient and light availability which support estuarine food web in addition to input from the coastal water during the flow.

Estimation of Annual Phytoplankton Primary Production in the Seine Estuary

As a function of the sampling site, the annual PPP ranged between 17.26 and 81.53 g C m^{-2} year^{-1}. By taking each surface area into account (Table 2), annual PPP represented a total of 6032 t C year^{-1} and a mean annual PPP of 64.75 g C m^{-2} year^{-1}. This annual PPP is low compared with the range of annual mean PPP reported for 45 estuaries by Boynton et al. (1982) varying from 19 to 547 g C m^{-2} year^{-1} with a mean of 190 g C m^{-2} year^{-1} or for the 1148 measurements recorded in 131 estuarine and coastal ecosystems (estuaries, fjords, bays, and lagoons) reported by Cloern et al. (2014), which ranged from −105 to 1890 g C m^{-2} year^{-1} with a mean of 225 g C m^{-2} year^{-1}. In this context, and according to the classification of Nixon (1995), the Seine estuary can be classified as an oligotrophic system (< 100 g C m^{-2} year^{-1}). However, our results showed a nutrient-independent system which cannot be classified like this, because an estuary is not poor in terms of nutrient concentrations but still present at low primary production. It seems that a low PPP is not necessarily representative of an oligotrophic system but sometimes of a dynamic and complex system. Indeed, a wide range of variability within or between ecosystems and estuaries, sampling effort and methods may explain this range. Some environmental dynamics like temperature or the level of irradiance

are determined by the geographic location or by bathymetric, hydrodynamic, or morphologic characteristics. We must therefore be wary when comparing the various estuarine systems. In the Seine estuary, the low PPP value is principally due to the intense turbidity. It is also important to note that we focused the sampling strategy on salinity gradient without considering the upper freshwater part of the estuary. PPP of this upper part can be high (Descy et al. 2017) and can considerably contribute to the estuarine trophic network in terms of POC (Etcheber et al. 2007). Sampling effort also explain a large part of the discrepancy of annual PPP estimations between worldwide estuaries. Some authors based their annual estimation on few sites (Vegter 1977; Mallin et al. 1993) or made over a period of a couple of months in spring or summer (Smith and Kemp 1995) and extrapolates their results over a year. In the present study, the spatial variability was taken into account with high-frequency measurements distributed all along the salinity gradient even in the less productive areas (MTZ) and during the less productive season (winter). Indeed, in our study, the four most downstream areas (sites 1 to 4) produced 5239 t C during the six more productive months (from April to September), which represent 87% of the total annual PPP. This trivial example highlights the limit of this type of classification strongly related to sampling strategy and effort.

Conclusion

The measurement and estimation methods presented in this paper improved the phytoplankton primary production estimation along the salinity gradient of a temperate estuary. The combination of high-frequency and traditional methods in relation with the environment dynamics has shown the possibility of making accurate estimation of PPP at small-scale in these highly dynamic systems, and could be applied more frequently in valuable ecosystems such as estuaries or coastal waters to apprehend their functioning. We pointed out a quite low variability of the $\varphi_{e,C}$ because of nutrient replete conditions which allow to use variable fluorescence technics (PAM, FRRf) to get accurate PPP in estuaries. Phytoplankton biodiversity analysis was also performed during this study; therefore, the relationship between biodiversity, community structures, and PPP will be explored in complement to this work.

References

Alderkamp, A.-C., H.J.W. de Baar, R.J.W. Visser, and K.R. Arrigo. 2010. Can photoinhibition control phytoplankton abundance in deeply mixed water columns of the Southern Ocean? *Limnology and Oceanography* 55 (3): 1248–1264. https://doi.org/10.4319/lo.2010.55.3.1248.

Aminot, A., and M. Chaussepied. 1983. *Manuel des analyses chimiques en milieu marin*, 395. Paris: Editions Jouve, CNEXO.

Aminot, A., and R. Kérouel. 2004. *Hydrologie des écosystèmes marins: paramètres et analyses. Méthodes d'analyse en milieu marin*, 336. Plouzané: Editions IFREMER.

Aminot, A., and R. Kérouel. 2007. Dosage automatique des nutriments dans les eaux marines: méthodes en flux continu. In *Méthodes d'analyse en milieu marin*, ed. Ifremer, 188.

Anning, T., H.L. Macintyre, S.M. Pratt, P.J. Sammes, S. Gibb, and R.J. Geider. 2000. Photoacclimation in the marine diatom Skeletonema costatum. *Limnology and Oceanography* 45 (8): 1807–1817. https://doi.org/10.4319/lo.2000.45.8.1807.

Babin, M., A. Morel, and R. Gagnon. 1994. An incubator designed for extensive and sensitive measurements phytoplankton photosynthetic parameters. *Limnology and Oceanography* 39: 694–702.

Babin, M., A. Morel, H. Claustre, A. Bricaud, Z. Kolber, and P.G. Falkowski. 1996. Nitrogen- and irradiance-dependent variations of the maximum quantum yield of carbon fixation in eutrophic, mesotrophic and oligotrophic marine systems. *Deep Sea Research* 43 (8): 1241–1272. https://doi.org/10.1016/0967-0637(96)00058-1.

Bailleul, B., N. Berne, O. Murik, D. Petroutsos, J. Prihoda, A. Tanaka, V. Villanova, R. Bligny, S. Flori, D. Falconet, A. Krieger-liszkay, S. Santabarbara, F. Rappaport, P. Joliot, L. Tirichine, P.G. Falkowski, P. Cardol, C. Bowler, and G. Finazzi. 2015. Mitochondria drives CO 2 assimilation in diatoms. *Nature* 524 (7565): 366–369. https://doi.org/10.1038/nature14599.

Barranguet, C., and J. Kromkamp. 2000. Estimating primary production rates from photosynthetic electron transport in estuarine microphytobenthos. *Marine Ecology Progress Series* 204: 39–52. https://doi.org/10.3354/meps204039.

Boynton, W., W. Kemp, and C. Keefe. 1982. A comparative analysis of nutrients and other factors influencing estuarine phytoplankton production. In *Estuarine Comparisons*, ed. V. S. Kennedy, 69–90. New York: Academic Press.

Brenon, I., and P. Le Hir. 1999. Modelling the turbidity maximum in the Seine estuary (France): identification of formation. *Estuarine, Coastal and Shelf Science* 49: 525–544.

Campbell, D.A., V. Hurry, A.K. Clarke, P. Gustafsson, and G. Oquist. 1998. Chlorophyll fluorescence analysis of cyanobacterial photosynthesis and acclimation. *Microbiology and Molecular Biology Reviews: MMBR* 62 (3): 667–683.

Chen, C.-T.A., and A.V. Borges. 2009. Reconciling opposing views on carbon cycling in the coastal ocean: continental shelves as sinks and near-shore ecosystems as sources of atmospheric CO2. *Deep Sea Research Part II: Topical Studies in Oceanography* 56 (8-10): 578–590. https://doi.org/10.1016/j.dsr2.2009.01.001.

Chessel, D., A.B. Dufour, and J. Thioulouse. 2004. The ade4 package - I: one-table methods. *R News* 4: 5–10.

Claquin, P., I. Probert, S. Lefebvre, and B. Veron. 2008. Effects of temperature on photosynthetic parameters and TEP production in eight species of marine microalgae. *Aquatic Microbial Ecology* 51: 1–11. https://doi.org/10.3354/ame01187.

Claquin, P., S.N.Í. Longphuirt, P. Fouillaron, P. Huonnic, O. Ragueneau, C. Klein, and A. Leynaert. 2010. Effects of simulated benthic fluxes on phytoplankton dynamic and photosynthetic parameters in a mesocosm experiment (Bay of Brest, France). *Estuarine, Coastal and Shelf Science* 86 (1): 93–101. https://doi.org/10.1016/j.ecss.2009.10.017.

Cloern, J.E. 1996. Phytoplankton bloom dynamics in coastal ecosystems: a review with some general lessons from sustained investigation of San Francisco Bay, California. *Reviews of Geophysics* 34 (2): 127–168. https://doi.org/10.1029/96RG00986.

Cloern, J.E., S.Q. Foster, and A.E. Kleckner. 2014. Phytoplankton primary production in the world's estuarine-coastal ecosystems. *Biogeosciences* 11 (9): 2477–2501. https://doi.org/10.5194/bg-11-2477-2014.

Davison, I.R. 1991. Environmental effects on algal photosynthesis: temperature. *Journal of Phycology* 27 (1): 2–8. https://doi.org/10.1111/j.0022-3646.1991.00002.x.

Descy, J.-P., F. Darchambeau, T. Lambert, M.P. Stoyneva-Gaertner, S. Bouillon, and A.V. Borges. 2017. Phytoplankton dynamics in the Congo River. *Freshwater Biology* 62 (1): 87–101.

Dortch, Q., and T.E. Whitledge. 1992. Does nitrogen or silicon limit phytoplankton production in the Mississippi River plume and nearby regions? *Continental Shelf Research* 12 (11): 1293–1309. https://doi.org/10.1016/0278-4343(92)90065-R.

Dray, S., and A.B. Dufour. 2007. The ade4 package: implementing the duality diagram for ecologists. *Journal of Statistical Software* 22: 1–20.

Dubinsky, Z., and N. Stambler. 2009. Photoacclimation processes in phytoplankton: mechanisms, consequences, and applications. *Aquatic Microbial Ecology* 56: 163–176. https://doi.org/10.3354/ame01345.

Eilers, P.H.C., and J.C.H. Peeters. 1988. A model for the relationship between light intensity and the rate of photosynthesis in phytoplankton. *Ecological Modelling* 42 (3-4): 199–215. https://doi.org/10.1016/0304-3800(88)90057-9.

Endo, T., and K. Asada. 2002. Photosystem I and photoprotection: cyclic electron flow and water-water cycle. In *Photoprotection, Photoinhibition, Gene Regulation and Environment*, ed. Demmin-Adams, B., Adams, W.W. III, and A.K. Matoo, 205–221. The Netherlands: Springer.

Etcheber, H., A. Taillez, G. Abril, J. Garnier, P. Servais, F. Moatar, and M.V. Commarieu. 2007. Particulate organic carbon in the estuarine turbidity maxima of the Gironde, Loire and Seine estuaries: origin and lability. *Hydrobiologia* 588 (1): 245–259. https://doi.org/10.1007/s10750-007-0667-9.

Even, S., J.M. Mouchel, P. Servais, N. Flipo, M. Poulin, S. Blanc, M. Chabanel, and C. Paffoni. 2007. Modelling the impacts of combined sewer overflows on the river Seine water quality. *Science of the Total Environment* 375 (1-3): 140–151. https://doi.org/10.1016/j.scitotenv.2006.12.007.

Falkowski, P.G., and J.A. Raven. 1997. *Aquatic photosynthesis*. Malden: Blackwell Science.

Garnier, J., G. Billen, J. Némery, and M. Sebilo. 2010. Transformations of nutrients (N, P, Si) in the turbidity maximum zone of the Seine estuary and export to the sea. *Estuarine, Coastal and Shelf Science* 90 (3): 129–141. https://doi.org/10.1016/j.ecss.2010.07.012.

Genty, B., J. Harbinson, J. Briantais, N.R. Baker, and C. Lane. 1989. The relationship between non-photochemical quenching of chlorophyll fluorescence and the rate of photosystem 2 photochemistry in leaves. *Photosynthesis Research* 25: 249–257.

Goosen, N.K., J. Kromkamp, J. Peene, P. Van Rijswijk, and P. Van Breugel. 1999. Bacterial and phytoplankton production in the maximum turbidity zone of three major European estuaries: the Elbe, Westerschelde and Gironde. *Journal of Marine Systems* 22 (2-3): 151–171. https://doi.org/10.1016/S0924-7963(99)00038-X.

Goss, R., and T. Jakob. 2010. Regulation and function of xanthophyll cycle-dependent photoprotection in algae. *Photosynthesis Research* 106 (1-2): 103–122. https://doi.org/10.1007/s11120-010-9536-x.

Hama, T., T. Miyazaki, Y. Ogawa, T. Iwakuma, M. Takahashi, A. Otsuki, and S. Ichimura. 1983. Measurement of photosynthetic production of a marine phytoplankton population using a stable 13C isotope. *Marine Biology* 73 (1): 31–36. https://doi.org/10.1007/BF00396282.

Hancke, K., T. Dalsgaard, M.K. Sejr, S. Markager, and R.N. Glud. 2015. Phytoplankton Productivity in an arctic fjord (West Greenland): estimating electron requirements for carbon fixation and oxygen production. *PLoS One* 10: 1–23.

Hartig, P., K. Wolfstein, S. Lippemeier, and F. Colijn. 1998. Photosynthetic activity of natural microphytobenthos populations measured by fluorescence (PAM) and 14C-tracer methods: a comparison. *Marine Ecology Progress Series* 166: 53–62. https://doi.org/10.3354/meps166053.

Hernando, M., I.R. Schloss, G. Malanga, G.O. Almandoz, G.A. Ferreyra, M.B. Aguiar, and S. Puntarulo. 2015. Effects of salinity changes on coastal Antarctic phytoplankton physiology and assemblage composition. *Journal of Experimental Marine Biology and Ecology* 466: 110–119. https://doi.org/10.1016/j.jembe.2015.02.012.

Holm-Hansen, O., A.F. Amos, and C.D. Hewes. 2000. Reliability of estimating chlorophyll a concentrations in Antarctic waters by measurement of in situ chlorophyll a fluorescence. *Marine Ecology Progress Series* 196: 103–110. https://doi.org/10.3354/meps196103.

Hunter-Cevera, K.R., M.G. Neubert, R.J. Olson, A.R. Solow, A. Shalapyonok, and H.M. Sosik. 2016. Physiological and ecological drivers of early spring blooms of a coastal phytoplankter. *Science* 354 (6310): 326–329. https://doi.org/10.1126/science.aaf8536.

Hydes, D., M. Aoyama, A. Aminot, K. Bakker, S. Becker, S. Coverly, A. Daniel, A.G. Dickson, O. Grosso, R. Kerouel, J. van Ooijen, K. Sato, T. Tanhua, E.M.S. Woodward, and J.Z. Zhang. 2010. Determination of dissolved nutrients (N, P, Si) in seawater with high precision and inter-comparability using gas-segmented continuous flow analysers. *The GO-SHIP Repeat Hydrography Manual IOCCP Report* 134: 1–87.

Johnsen, G., and E. Sakshaug. 2007. Biooptical characteristics of PSII and PSI in 33 species (13 pigment groups) of marine phytoplankton, and the relevance for pulse-amplitude-modulated and fast-repetition-rate fluorometry 1. *Journal of Phycology* 43 (6): 1236–1251. https://doi.org/10.1111/j.1529-8817.2007.00422.x.

Johnson, X., and J. Alric. 2013. Central carbon metabolism and electron transport in chlamydomonas reinhardtii: Metabolic constraints for carbon partitioning between oil and starch. *Eukaryotic Cell* 12 (6): 776–793. https://doi.org/10.1128/EC.00318-12.

Jouenne, F., S. Lefebvre, B. Véron, and Y. Lagadeuc. 2007. Phytoplankton community structure and primary production in small intertidal estuarine-bay ecosystem (eastern English Channel, France). *Marine Biology* 151 (3): 805–825. https://doi.org/10.1007/s00227-006-0440-z.

Juneau, P., and P. J. Harrison. 2005. Comparison by PAM fluorometry of photosynthetic activity of nine marine phytoplankton grown under identical conditions. photochemistry and photobiology, 649–653.

Kaiblinger, C., and M.T. Dokulil. 2006. Application of fast repetition rate fluorometry to phytoplankton photosynthetic parameters in freshwaters. *Photosynthesis Research* 88 (1): 19–30. https://doi.org/10.1007/s11120-005-9018-8.

Kimmerer, W.J., A.E. Parker, U.E. Lidström, and E.J. Carpenter. 2012. Short-term and interannual variability in primary production in the low-salinity zone of the San Francisco estuary. *Estuaries and Coasts* 35 (4): 913–929. https://doi.org/10.1007/s12237-012-9482-2.

Klughammer, C., and U. Schreiber. 2015. Apparent PS II absorption cross-section and estimation of mean PAR in optically thin and dense suspensions of Chlorella. *Photosynthesis Research* 123 (1): 77–92. https://doi.org/10.1007/s11120-014-0040-6.

Kolber, Z., and P.G. Falkowski. 1993. Use of active fluorescence to estimate phytoplankton photosynthesis in situ. *Limnology and Oceanography* 38 (8): 1646–1665. https://doi.org/10.4319/lo.1993.38.8.1646.

Kolber, Z.S., O. Prášil, and P.G. Falkowski. 1998. Measurements of variable chlorophyll fluorescence using fast repetition rate techniques: defining methodology and experimental protocols. *Biochimica et*

Biophysica Acta - Bioenergetics 1367 (1-3): 88–106. https://doi.org/10.1016/S0005-2728(98)00135-2.

Kromkamp, J.C., and R.M. Forster. 2003. The use of variable fluorescence measurements in aquatic ecosystems: differences between multiple and single turnover measuring protocols and suggested terminology. *European Journal of Phycology* 38 (2): 103–112. https://doi.org/10.1080/0967026031000094094.

Kromkamp, J.C., and J. Peene. 2005. Changes in phytoplankton biomass and primary production between 1991 and 2001 in the Westerschelde estuary (Belgium/The Netherlands). *Hydrobiologia* 540 (1-3): 117–126. https://doi.org/10.1007/s10750-004-7124-9.

Lawrenz, E., G. Silsbe, E. Capuzzo, P. Ylöstalo, R.M. Forster, S.G.H. Simis, O. Prášil, J.C. Kromkamp, A.E. Hickman, C.M. Moore, M.-H. Forget, R.J. Geider, and D.J. Suggett. 2013. Predicting the electron requirement for carbon fixation in seas and oceans. *PLoS One* 8 (3): e58137. https://doi.org/10.1371/journal.pone.0058137.

Lionard, M., K. Muylaert, D. Van Gansbeke, and W. Vyverman. 2005. Influence of changes in salinity and light intensity on growth of phytoplankton communities from the Schelde river and estuary (Belgium/The Netherlands). *Hydrobiologia* 540 (1-3): 105–115. https://doi.org/10.1007/s10750-004-7123-x.

Lohrenz, S.E., G.L. Fahnenstiel, D.G. Redalje, G.A. Lang, M.J. Dagg, T.E. Whitledge, and Q. Dortch. 1999. Nutrients, irradiance, and mixing as factors regulating primary production in coastal waters impacted by the Mississippi River plume. *Continental Shelf Research* 19 (9): 1113–1141. https://doi.org/10.1016/S0278-4343(99)00012-6.

Lorenzen, C.J. 1966. A method for the continuous measurement of in vivo chlorophyll concentration. *Deep Sea Research and Oceanographic Abstracts* 13 (2): 223–227. https://doi.org/10.1016/0011-7471(66)91102-8.

Macintyre, H.L., T.M. Kana, T. Anning, and R.J. Geider. 2002. Review Photoacclimation of photosynthesis irradiance response curves and photosynthetic pigments in microalgae and cyanobacteria. *Journal of Phycology* 38 (1): 17–38. https://doi.org/10.1046/j.1529-8817.2002.00094.x.

Magnien, R.E., R.M. Summers, and K.G. Sellner. 1992. External nutrient sources, internal nutrient pools, and phytoplankton production in Chesapeake Bay. *Estuaries* 15 (4): 497. https://doi.org/10.2307/1352393.

Mallin, M.A., H.W. Paerl, J. Rudek, and P.W. Bates. 1993. Regulation of estuarine primary production by watershed rainfall and river flow. *Marine Ecology Progress Series* 93: 199–203. https://doi.org/10.3354/meps093199.

Masojidek, J., J. Grobbelaar, L. Pechar, and M. Koblizek. 2001. Photosystem II electron transport rates and oxygen production in natural waterblooms of freshwater cyanobacteria during a diel cycle. *Journal of Plankton Research* 23 (1): 57–66. https://doi.org/10.1093/plankt/23.1.57.

Milligan, A.J., K.H. Halsey, and M.J. Behrenfeld. 2014. HORIZONS: advancing interpretations of 14C-uptake measurements in the context of phytoplankton physiology and ecology. *Journal of Plankton Research* 37: 692–698.

Morris, E.P., and J.C. Kromkamp. 2003. Influence of temperature on the relationship between oxygen- and fluorescence-based estimates of photosynthetic parameters in a marine benthic diatom (Cylindrotheca closterium). *European Journal of Phycology* 38 (2): 133–142. https://doi.org/10.1080/0967026031000085832.

Morris, A.W., A.J. Bale, and R.J.M. Howland. 1981. Nutrient distributions in an estuary: Evidence of chemical precipitation of dissolved silicate and phosphate. *Estuarine, Coastal and Shelf Science* 12 (2): 205–216. https://doi.org/10.1016/S0302-3524(81)80097-7.

Napoléon, C., and P. Claquin. 2012. Multi-parametric relationships between PAM measurements and carbon incorporation, an in situ approach. *PLoS One* 7: 1–12.

Napoléon, C., V. Raimbault, L. Fiant, P. Riou, S. Lefebvre, L. Lampert, and P. Claquin. 2012. Spatiotemporal dynamics of physicochemical and photosynthetic parameters in the central English Channel. *Journal of Sea Research* 69: 43–52. https://doi.org/10.1016/j.seares.2012.01.005.

Napoléon, C., L. Fiant, V. Raimbault, and P. Claquin. 2013a. Study of dynamics of phytoplankton and photosynthetic parameters using opportunity ships in the western English Channel. *Journal of Marine Systems* 128: 146–158. https://doi.org/10.1016/j.jmarsys.2013.04.019.

Napoléon, C., V. Raimbault, and P. Claquin. 2013b. Influence of nutrient stress on the relationships between PAM measurements and carbon incorporation in four phytoplankton species. *PLoS One* 8 (6): e66423. https://doi.org/10.1371/journal.pone.0066423.

Napoléon, C., L. Fiant, V. Raimbault, P. Riou, and P. Claquin. 2014. Dynamics of phytoplankton diversity structure and primary productivity in the English Channel. *Marine Ecology Progress Series* 505: 49–64. https://doi.org/10.3354/meps10772.

Némery, J., and J. Garnier. 2007. Origin and fate of phosphorus in the Seine watershed (France): Agricultural and hydrographic P budgets. *Journal of Geophysical Research: Biogeosciences* 112: 1–14.

Ning, X., D. Vaulot, Z. Liu, and Z. Liu. 1988. Standing stock and production of phytoplankton in the estuary of the Chang-jiang (Yangste River) and the adjacent East China Sea. *Marine Ecology Progress Series* 49: 141–150. https://doi.org/10.3354/meps049141.

Nixon, S.W. 1995. Coastal marine eutrophication: a definition, social causes, and future concerns. *Ophelia* 41 (1): 199–219. https://doi.org/10.1080/00785236.1995.10422044.

Nogales, J., S. Gudmundsson, E.M. Knight, B.O. Palsson, and I. Thiele. 2011. Detailing the optimality of photosynthesis in cyanobacteria through systems biology analysis. *PNAS* 109: 2678–2683.

Pannard, A., P. Claquin, C. Klein, B. Le Roy, and B. Véron. 2008. Short-term variability of the phytoplankton community in coastal ecosystem in response to physical and chemical conditions' changes. *Estuarine, Coastal and Shelf Science* 80 (2): 212–224. https://doi.org/10.1016/j.ecss.2008.08.008.

Parizzi, R.A., E. Da, C. Machado, C. Prestes, D. Santos, L.F. Fernandes, M.G. De Camargo, L. Laureno, and M. Jr. 2016. Primary productivity and phytoplankton dynamics in a subtropical estuary: a multiple timescale approach. *Scientia Marina* 80: 1–13.

Parkhill, J.P., G. Maillet, and J.J. Cullen. 2001. Fluorescence-based maximal quantum yield for PSII as a diagnostic of nutrient stress. *Journal of Phycology* 37 (4): 517–529. https://doi.org/10.1046/j.1529-8817.2001.037004517.x.

Passy, P., R. Le Gendre, J. Garnier, P. Cugier, J. Callens, F. Paris, G. Billen, P. Riou, and E. Romero. 2016. Eutrophication modelling chain for improved management strategies to prevent algal blooms in the Bay of Seine. *Marine Ecology Progress Series* 543: 107–125. https://doi.org/10.3354/meps11533.

Pauly, D., and V. Christensen. 1995. Primary production required to sustain global fisheries. 374: 255–257.

Pennock, J., and J. Sharp. 1986. Phytoplankton production in the Delaware Estuary: temporal and spatial variability. *Marine Ecology Progress Series* 34: 143–155. https://doi.org/10.3354/meps034143.

Sanford, L.P., S.E. Suttles, and J.P. Halka. 2001. Reconsidering the physics of the Chesapeake Bay estuarine turbidity maximum. *Estuaries* 24 (5): 655. https://doi.org/10.2307/1352874.

Schreiber, U., U. Schliwa, and W. Bilger. 1986. Continuous recording of photochemical and non-photochemical chlorophyll fluorescence quenching with a new type of modulation fluorometer. *Photosynthesis Research* 10 (1-2): 51–62. https://doi.org/10.1007/BF00024185.

Schreiber, U., C. Klughammer, and J. Kolbowski. 2012. Assessment of wavelength-dependent parameters of photosynthetic electron transport with a new type of multi-color PAM chlorophyll fluorometer.

Photosynthesis Research 113 (1-3): 127–144. https://doi.org/10.1007/s11120-012-9758-1.

Schuback, N., C. Schallenberg, C. Duckham, M.T. Maldonado, and P.D. Tortell. 2015. Interacting effects of light and iron availability on the coupling of photosynthetic electron transport and CO2-assimilation in marine phytoplankton. *PLoS One* 10 (7): e0133235. https://doi.org/10.1371/journal.pone.0133235.

Servais, P., and J. Garnier. 2006. Organic carbon and bacterial heterotrophic activity in the maximum turbidity zone of the Seine estuary (France). *Aquatic Sciences* 68 (1): 78–85. https://doi.org/10.1007/s00027-005-0809-y.

Sferratore, A., J. Garnier, G. Billen, D.J. Conley, and S. Pinault. 2006. Diffuse and point sources of silica in the Seine River Watershed. *Environmental Science and Technology* 40 (21): 6630–6635. https://doi.org/10.1021/es060710q.

Sharp, J.H., C.H. Culberson, and T.M. Church. 1982. The chemistry of the Delaware estuary. General considerations. *Limnology and Oceanography* 27 (6): 1015–1028. https://doi.org/10.4319/lo.1982.27.6.1015.

Shaw, P.J., and D.A. Purdie. 2001. Phytoplankton photosynthesis-irradiance parameters in the near-shore UK coastal waters of the North Sea: temporal variation and environmental control. *Marine Ecology Progress Series* 216: 83–94. https://doi.org/10.3354/meps216083.

Shelly, K., P. Heraud, J. Beardall, and E.T. Al. 2003. NOTE interactive effects of PAR and UV-b radiation on PSII electron transport in the marine alga dunaliella tertiolecta (chlorophyceae) to better understand the interactions between PAR and UV-B radiation in microalgae. *Journal of Phycology* 512: 509–512.

Smith, E.M., and W.M. Kemp. 1995. Seasonal and regional variations in plankton community production and respiration for Chesapeake Bay. *Marine Ecology Progress Series* 116: 217–232. https://doi.org/10.3354/meps116217.

Sorokin, Y.I., and P.Y. Sorokin. 1996. Plankton and primary production in the Lena River estuary and in the south-eastern Laptev Sea. *Estuarine, Coastal and Shelf Science* 43 (4): 399–418. https://doi.org/10.1006/ecss.1996.0078.

Suggett, D.J., H.L. MacIntyre, and R.J. Geider. 2004. Evaluation of bio-physical and optical determinations of light absorption by photosystem II in phytoplankton. *Limnology and Oceanography: Methods* 2 (10): 316–332. https://doi.org/10.4319/lom.2004.2.316.

Tillmann, U., K.-J. Hesse, and F. Colijn. 2000. Planktonic primary production in the German Wadden Sea. *Journal of Plankton Research* 22 (7): 1253–1276. https://doi.org/10.1093/plankt/22.7.1253.

Underwood, G.J.C., and J. Kromkamp. 1999. Primary production by phytoplankton and microphytobenthos in estuaries. *Advances in Ecological Research* 29: 93–153. https://doi.org/10.1016/S0065-2504(08)60192-0.

van Spaendonk, J.C.M., J.C. Kromkamp, and P.R.M. de Visscher. 1993. Primary production of phytoplankton in a turbid coastal plain estuary, the Westerschelde (The Netherlands). *Netherlands Journal of Sea Research* 31 (3): 267–279. https://doi.org/10.1016/0077-7579(93)90027-P.

Vegter, F. 1977. The closure of the grenvelingen estuary: its influence on phytoplankton primary production and nutrient content. *Hydrology* 52 (1): 67–71. https://doi.org/10.1007/BF02658083.

Verney, R., R. Lafite, and J.C. Brun-Cottan. 2009. Flocculation potential of estuarine particles: The importance of environmental factors and of the spatial and seasonal variability of suspended particulate matter. *Estuaries and Coasts* 32 (4): 678–693. https://doi.org/10.1007/s12237-009-9160-1.

Wang, Z.B., M.C.J.L. Jeuken, H. Gerritsen, H.J. De Vriend, and B.A. Kornman. 2002. Morphology and asymmetry of the vertical tide in the Westerschelde estuary. *Continental Shelf Research* 22 (17): 2599–2609. https://doi.org/10.1016/S0278-4343(02)00134-6.

Zhu, Y., J. Ishizaka, S.C. Tripathy, S. Wang, Y. Mino, T. Matsuno, and D.J. Suggett. 2016. Variation of the photosynthetic electron transfer rate and electron requirement for daily net carbon fixation in Ariake Bay, Japan. *Journal of Oceanography* 72 (5): 761–776. https://doi.org/10.1007/s10872-016-0370-4.